Torque Vectoring Control for Enhancing Vehicle Safety and Energy Efficiency

Basilio Lenzo

Abstract Torque vectoring control is one of the most interesting techniques applicable to electric vehicles with multiple motors. Essentially it is the possibility to allocate desired amounts of torque to each motor. With an uneven allocation of torque between left and right sides of the vehicle, a direct yaw moment can be generated and exploited to enhance the vehicle handling behaviour. This allows to enhance vehicle safety, stability and cornering performance. Significant energy efficiency benefits are also achievable, either as a main priority or as a secondary objective when the main target is the vehicle handling behaviour. This Chapter explains the underlying principles of each element of a torque vectoring control framework: reference generator, high level controller, and low level controller. Notable applications are also presented and discussed in detail.

1 Introduction

In general, torque vectoring can be defined as a feature that allows to control torque at individual wheel level. The most frequent reason for employing torque vectoring is the improvement of vehicle longitudinal and/or lateral dynamics (Esmailzadeh et al., 2003; Lenzo et al., 2019b)—hence affecting vehicle safety, stability and cornering performance. This is normally achieved by allocating different amounts of torque to the left side and right side of a vehicle, resulting in the generation of a yaw moment at vehicle level—it is not uncommon to see the concepts of direct yaw moment control (DYC) and torque vectoring used interchangeably, even if actually the former is achievable through a specific use of the latter. Torque vectoring can also be used to

B. Lenzo (✉)
Department of Industrial Engineering, University of Padova, Padova, Italy
e-mail: basilio.lenzo@unipd.it

Department of Engineering and Mathematics, Sheffield Hallam University, Sheffield, UK

B. Lenzo (ed.), *Vehicle Dynamics*, CISM International Centre for Mechanical Sciences 603, https://doi.org/10.1007/978-3-030-75884-4_4

enhance energy efficiency in electric vehicles (Sforza et al., 2019; De Filippis et al., 2016, 2021).

Based on the above definition, in some sense torque vectoring is already implemented in modern passenger cars. In fact, these are equipped with Anti-lock Braking System (ABS) and Electronic Stability Control (ESC), that control friction braking torques on individual wheels when safety-critical conditions are detected. However, this individual wheel torque control is limited to braking torques, i.e. a standard passenger car cannot control individual traction torques. Cars are normally equipped with a single source of power (very often that is an internal combustion engine) and an open differential, which implies that the torque is evenly distributed between left and right side of a driven axle (Guiggiani, 2018).

A way to achieve torque vectoring for traction torques is the use of appropriate mechanical systems, including limited slip differentials or more complex systems known as torque vectoring systems (TVS, Piyabongkarn et al., 2010). Despite being effective, often these approaches have limitations including the impossibility to allocate more torque on the faster wheel of the axle (in case of limited slip differentials) and/or the inability to achieve a left-right torque bias in certain driving conditions, such as off-throttle situations.

Torque vectoring can be achieved, by definition, in electric vehicles with multiple motors. In this case the constraints of mechanical systems are overcome, i.e., it is possible to allocate more torque to the faster wheel of an axle, and it is possible to achieve a left-right torque bias even when the overall vehicle torque demand is zero. Clearly, there are still intrinsic constraints, for example the amount of left-right torque bias is limited by the torque characteristics of the available motors and the vehicle layout. Figure 1 shows a schematic of a vehicle layout featuring four on-board motors, while other layouts are investigated, e.g., in De Novellis et al. (2014a) and Tuncay et al. (2011).

Consistently with the focus of this book on future trends, this Chapter explores torque vectoring techniques for electric vehicles with multiple motors. Here, interestingly, torque vectoring may be continuously active to provide consistent vehicle dynamics benefits, which is an important difference with respect to traditional control systems such as ABS and ESC.

2 Torque Vectoring Control Framework

The majority of the literature agree that a torque vectoring control framework is composed by three main blocks (Fig. 2):

Reference generator
The reference generator (Sect. 3) combines information on measured/estimated vehicle states and on the driver input, thereby generating reference values for relevant vehicle quantities. Normally these are a reference yaw rate, r_{ref}, and in some cases

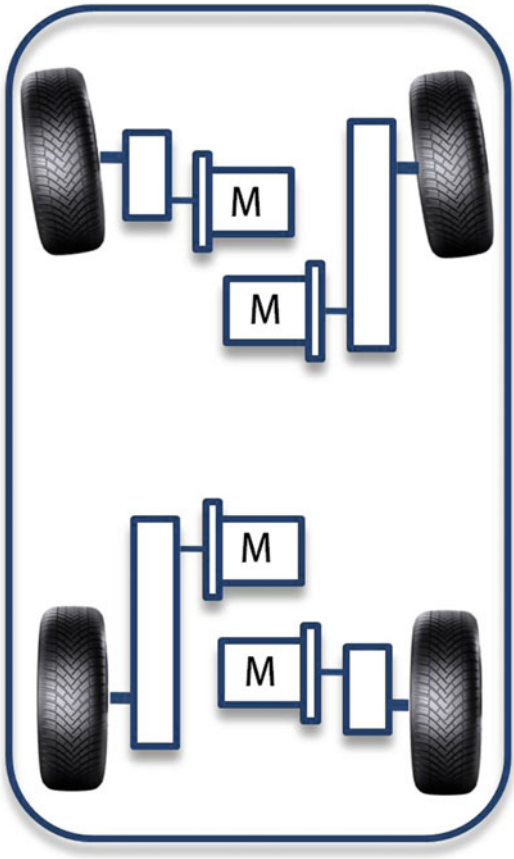

Fig. 1 Schematic of vehicle layout with four independent motors. In this example the on-board configuration requires appropriate gear transmissions to reach the wheels, as opposed to an in-wheel motor configuration

a reference sideslip angle, β_{ref}. Such reference(s), to be followed by the vehicle through torque vectoring, are given as input to the high level controller.

High level controller
The high level controller (Sect. 4) takes the output target quantities from the reference generator, as well as the driver input (e.g. accelerator/brake pedal positions) and vehicle states (e.g. vehicle velocity). Such inputs are elaborated to compute the desired total torque T_{tot} and yaw moment M_z to be applied at the vehicle level.

Low level controller
The task of the low level controller (Sect. 5) is to map the desired total torque and yaw moment into values of torque demand for each motor. Considering a typical electric vehicle layout featuring four motors, there are potentially four degrees of freedom (DOF), i.e. the four values of torque that can be assigned, T_{ij}, where $i = 1, 2$ respectively for front and rear, $j = 1, 2$ respectively for left and right. Since T_{tot} and M_z are imposed by the high level controller, practically there are only two available

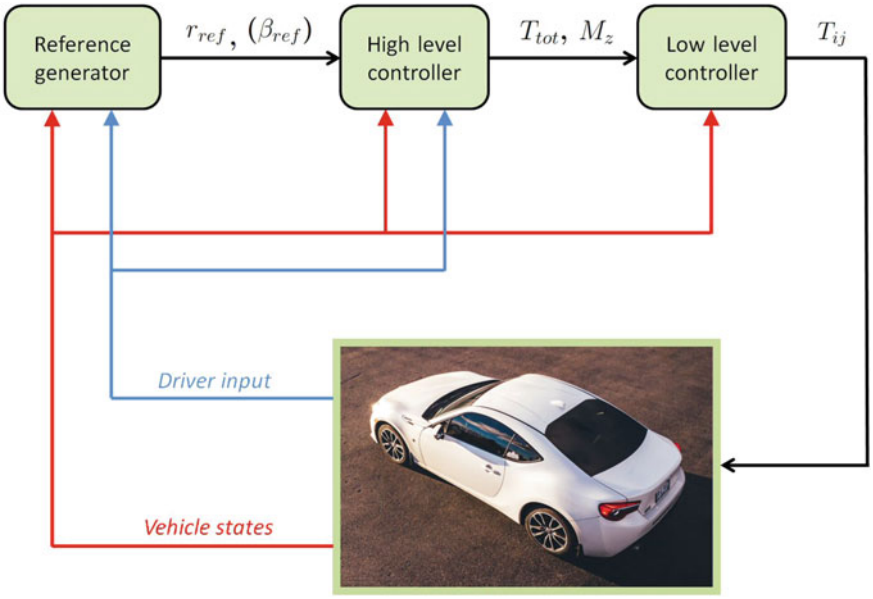

Fig. 2 Typical layout of a torque vectoring control framework

DOF. In other words, the desired total torque and yaw moment can be achieved with virtually ∞^2 combinations of the four motor torques. Relevant vehicle states (e.g. vehicle velocity), along with physical constraints (e.g. nominal motor torque), may be used to determine the most appropriate combination.

The underlying principles of the three blocks, as well as some notable applications, are covered in the remainder. Where relevant, the Adapted ISO sign convention (Pacejka, 2006) is adopted.

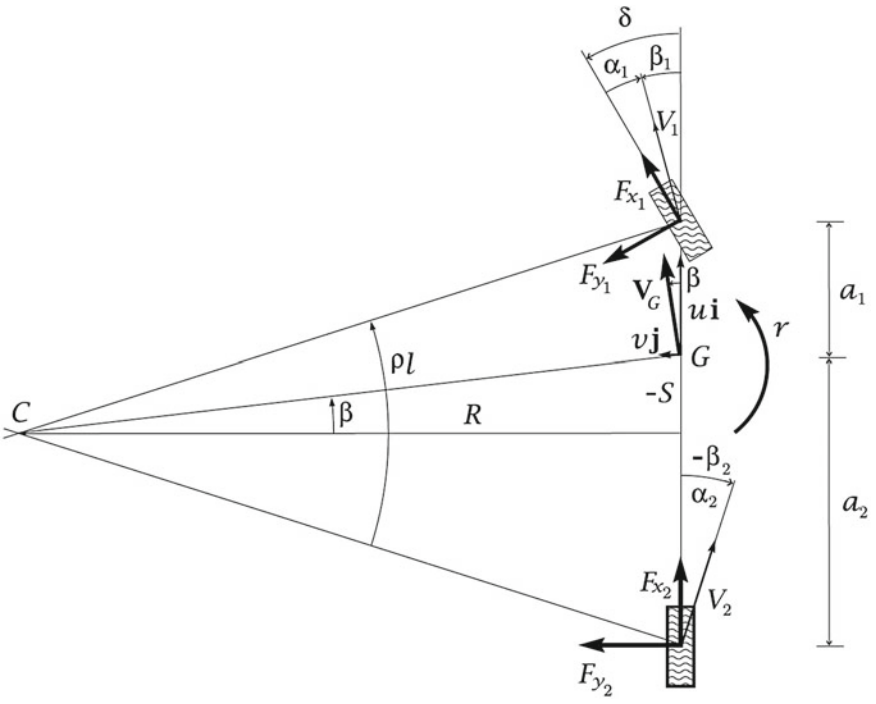

Fig. 3 Single-track vehicle model (adapted from Guiggiani, 2018)

3 Reference Generator: r_{ref}, (β_{ref})

In light of the above, this Section first focuses on the generation of a reference yaw rate. The concurrent control of yaw rate and sideslip angle is dealt with in Sect. 3.3.

3.1 Fundamentals on the Design of r_{ref}

The reference yaw rate is defined based on a simple principle, that is the redesign of the vehicle cornering response. This concept is elaborated hereinafter.

As well-known, for a single-track vehicle model with no rear wheel steering (Fig. 3) the congruence relationships (Lenzo & De Castro, 2019) are:

$$\alpha_1 = \delta - \beta_1 \tag{1}$$

$$\alpha_2 = -\beta_2 \tag{2}$$

where α_1 and α_2 are respectively the apparent slip angles of the front and rear axle, δ is the wheel steer angle, β_1 and β_2 are respectively the sideslip angle at the front and rear axle centre. Owing to the classical hypothesis of car assumed as a rigid body in planar motion, and small sideslip angles,

$$\beta_1 = \arctan \frac{v + ra_1}{u} \approx \frac{v + ra_1}{u} \approx \beta + \frac{ra_1}{u} \tag{3}$$

$$\beta_2 = \arctan \frac{v - ra_2}{u} \approx \frac{v - ra_2}{u} \approx \beta - \frac{ra_2}{u} \tag{4}$$

where u and v are respectively the longitudinal and lateral components of the velocity of the vehicle centre of mass, a_1 and a_2 are respectively the vehicle front and rear semi-wheelbases, r is the vehicle yaw rate (often also indicated with $\dot{\psi}$), $\beta = \arctan(v/u)$ is the vehicle sideslip angle (also known as vehicle slip angle). Therefore:

$$\alpha_1 \approx \delta - \beta - \frac{ra_1}{u} \tag{5}$$

$$\alpha_2 \approx -\beta + \frac{ra_2}{u} \tag{6}$$

Subtracting 6 from 5:

$$\delta = \frac{r(a_1 + a_2)}{u} + \alpha_1 - \alpha_2 \tag{7}$$

which can be rewritten as

$$\delta = \frac{l}{R} + \alpha_1 - \alpha_2 \tag{8}$$

where $l = a_1 + a_2$ is the vehicle wheelbase and $R = u/r$ is, formally, the lateral coordinate of the vehicle instant centre (point C in Fig. 3), which is often confused with the vehicle radius of curvature.[1] Although instant centre and centre of curvature do not coincide in general (Guiggiani, 2018), they do in some cases, including steady-state conditions. Using a linear tyre model, the expressions of α_1 and α_2 can be replaced by the constitutive equations:

$$\alpha_1 = \frac{F_{y_1}}{C_1} \tag{9}$$

$$\alpha_2 = \frac{F_{y_2}}{C_2} \tag{10}$$

where F_{y_1} and F_{y_2} are respectively the front and rear axle lateral forces, and C_1 and C_2 are respectively the front and rear axle cornering stiffness values.

[1] Also, sometimes R is confused with the distance between instant centre and centre of mass $\frac{\sqrt{u^2+v^2}}{r}$ (or simply CG in Fig. 3), this is fine for small values of v.

The equilibrium equations of the single-track model read:

$$F_{y_1} + F_{y_2} = ma_y \tag{11}$$

$$F_{y_1} a_1 - F_{y_2} a_2 = J_z \dot{r} \tag{12}$$

where m is the vehicle mass, J_z the vehicle moment of inertia with respect to a vertical axis through the centre of mass, a_y the vehicle lateral acceleration.

In steady-state conditions $\dot{r} = 0$ and $a_y = \dot{v} + ur = ur$, so from 11 and 12, F_{y_1} and F_{y_2} can be obtained as:

$$F_{y_1} = \frac{ma_y a_2}{l} \tag{13}$$

$$F_{y_2} = \frac{ma_y a_1}{l} \tag{14}$$

Finally, by replacing this result in 8 together with 9 and 10:

$$\delta = \frac{l}{R} + \frac{m(C_2 a_2 - C_1 a_1)}{l C_1 C_2} a_y \tag{15}$$

which is often written as:

$$\delta = \frac{l}{R} + K l a_y \tag{16}$$

where K is the understeer coefficient, or understeer gradient:

$$K = \frac{m(C_2 a_2 - C_1 a_1)}{l^2 C_1 C_2} \tag{17}$$

Note that the definition of K given above corresponds to the "stability factor" in Genta (1997) and differs from the more classical definition, K_{us}, by a factor l:

$$K_{us} = \frac{m(C_2 a_2 - C_1 a_1)}{l C_1 C_2} \tag{18}$$

which would produce

$$\delta = \frac{l}{R} + K_{us} a_y \tag{19}$$

instead of 16. A very interesting approach to the definition of understeer is given in Guiggiani (2018), which coincides with 17 in case of linear tyres. The interested reader may also look at Bucchi and Frendo (2016); Lenzo et al. (2019a) for another definition of the understeer coefficient.

Remarkably, 16 and 19 can be written in the form:

$$\delta = \delta_{kin} + \delta_{dyn} \tag{20}$$

where δ_{kin} is denoted as kinematic wheel steer angle (also known as Ackermann angle):

$$\delta_{kin} = \frac{l}{R} \tag{21}$$

and δ_{dyn} is denoted as dynamic wheel steer angle:

$$\delta_{dyn} = K_{us} a_y = K l a_y \tag{22}$$

Note that similar definitions could be provided in terms of the steering wheel angle δ_{sw}:

$$\delta_{sw} = \delta_{sw,kin} + \delta_{sw,dyn} \tag{23}$$

where $\delta_{sw,kin}$ is the kinematic steering wheel angle and $\delta_{sw,dyn}$ is the dynamic steering wheel angle. The relationship between δ_{sw} and δ can be expressed by a suitable map (an example of map is shown in Lenzo et al. (2019a)) or, when appropriate, it can be simplified as a factor called steering ratio, S_r: $\delta_{sw} = S_r \delta$.[2]

The relationship between $\delta_{sw,dyn}$ (or δ_{dyn}) and a_y is known as the vehicle cornering response, or vehicle understeer characteristic, which is the design target. Equation 16 can be rewritten as:

$$\delta = \frac{rl}{u} + Klur \tag{24}$$

which, solving for r, provides a formulation for the reference yaw rate:

$$r_{ref} = \frac{u}{l(Ku^2 + 1)} \delta \tag{25}$$

This approach to design the vehicle cornering response is used by many authors, that simply use the understeer gradient as a tuning parameter (Siampis et al., 2016; Esmailzadeh et al., 2003; De Novellis et al., 2013; Koehler et al., 2015; Wong et al., 2016; Vignati et al., 2016; Ding et al., 2017; Parra et al., 2018), although with slight differences such as the use of:

- different symbols for the same quantities;
- different definitions of understeer gradient, very often K_{us}, sometimes K;
- the total vehicle velocity V instead of u as they are nearly the same for small sideslip angles ($u = V \cos \beta$);
- the steering wheel angle δ_{sw} instead of the wheel steer angle δ.

[2] S_r may be roughly between 12 and 20.

In any case the understeer gradient is chosen to be positive. That implies an understeering behaviour, which in a standard vehicle is preferred to oversteer for safety reasons. Finally, it should be considered that normally:

- the reference yaw rate obtained via 25 is saturated, for example Ding et al. (2017) and Rajamani (2011) suggest:

$$|r_{ref,MAX}| = 0.85\frac{\mu g}{V} \tag{26}$$

  where μ is the estimated available tyre-road friction coefficient, and g is the gravitational acceleration;
- a first order lag is applied to r_{ref} to provide a smoothing action, i.e., in the Laplace domain the actual reference yaw rate is:

$$r_{ref,actual}(s) = \frac{r_{ref}}{\tau_1 s + 1} \tag{27}$$

  where s is the Laplace operator and τ_1 a suitable time constant.

A more comprehensive approach to the definition of the desired understeer characteristic is described in the following section.

3.2 *Design of the Full Vehicle Cornering Response and Driving Modes*

The method shown in 25 implies a simple linear relationship between dynamic steering angle and lateral acceleration. However this is only an approximation of a real vehicle behaviour, accurate only for low values of a_y, as shown e.g. in Fig. 4. It would then seem natural to go beyond the mere design of a tuning coefficient, by actually designing the whole understeer characteristic of the vehicle—so as to replicate a realistic shape. Although in principle any profile might be chosen, the designer should aim for a cornering response with clear benefits with respect to the baseline vehicle but not excessively far from it, to avoid unnatural vehicle behaviour. It should also be considered that too large deviations from the behaviour of the baseline vehicle may require a too severe control action which might not be practically achievable by the torque vectoring controller, due to physical limits on the maximum M_z.

Figure 4 shows a typical understeer characteristic and a potential characteristic achievable by torque vectoring. Desirable targets of the design of the understeer characteristic include: (i) increase of the steering responsiveness of the vehicle; (ii) extension of the region of linear cornering response; (iii) increase of the maximum lateral acceleration. In particular, De Novellis et al. (2014a) propose a piecewise function as the relationship between dynamic steering wheel angle and lateral acceleration[3]:

[3] Again the sideslip angle is assumed small so that $V \approx u$.

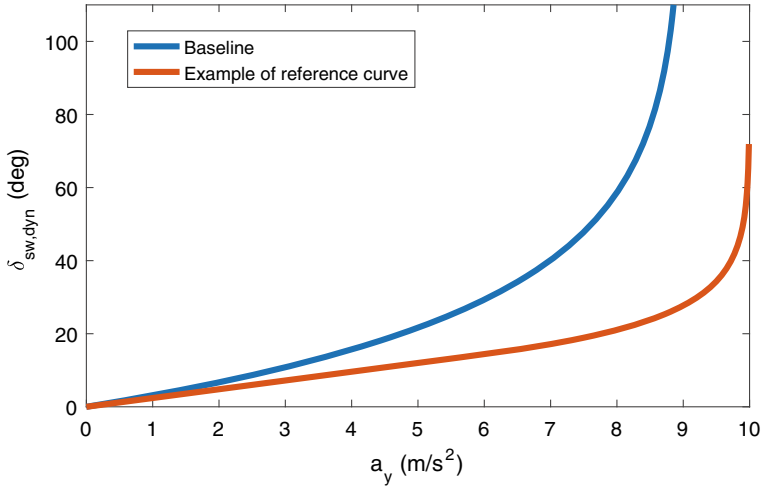

Fig. 4 Examples of vehicle cornering response: baseline curve and a potential reference curve with reduced understeer gradient, extended linear region (up until $a_y^* = 7$ m/s^2), increased maximum lateral acceleration ($a_{y,MAX} = 10$ m/s^2)

$$a_y = \begin{cases} \dfrac{1}{K_{us}\delta_{sw,dyn}} & \text{if } \delta_{sw,dyn} \leq a_y^* K_{us} \\ a_{y,MAX} + \left(a_y^* - a_{y,MAX}\right) e^{\frac{K_{us}a_y^* - \delta_{sw,dyn}}{(a_{y,MAX} - a_y^*)K_{us}}} & \text{if } \delta_{sw,dyn} > a_y^* K_{us} \end{cases} \tag{28}$$

which addresses the aforementioned desirable targets by allowing to tune three parameters:

- K_{us}, already defined, represents the initial slope of the curve. For instance, a value of K_{us} lower than for the baseline vehicle results in a more reactive vehicle (closer to a neutral behaviour).
- a_y^* is the lateral acceleration limit of the linear region.
- $a_{y,MAX}$ is the maximum achievable lateral acceleration.

The maximum lateral acceleration $a_{y,MAX}$ depends on the estimated available tyre-road friction coefficient, μ, and on the longitudinal acceleration, a_x.[4] Practically, $a_{y,MAX}$ can be computed either from a g-g diagram considering semi-axes $\approx \mu g$ (where g is the gravitational acceleration) or through the friction ellipse approach (Genta, 1997) based on the knowledge of a_x and the maximum achievable force obtained through a tyre model (which needs a reasonable estimate of μ), as discussed in Mangia et al. (2021). It is worth to mention that $a_{y,MAX}$ is typically limited to $\approx 9 - 10$ m/s^2 in normal conditions (dry asphalt), but it might be larger in specific cases, e.g. high quality tarmac, special tyres, etc.

[4] The effect of a_x on the cornering response can be seen in De Novellis et al. (2015a), Figs. 6 and 7.

An intuitive explanation of the possibility to increase the maximum lateral acceleration is given as follows. By considering again the equilibrium equations of the single-track model 11 and 12, this time accounting for the presence of a direct yaw moment M_z:

$$F_{y_1} + F_{y_2} = ma_y \tag{29}$$

$$F_{y_1} a_1 - F_{y_2} a_2 + M_z = J_z \dot{r} \tag{30}$$

By solving for F_{y_1} and F_{y_2} in steady-state conditions:

$$F_{y_1} = \frac{ma_y a_2}{l} - \frac{M_z}{l} \tag{31}$$

$$F_{y_2} = \frac{ma_y a_1}{l} + \frac{M_z}{l} \tag{32}$$

As discussed earlier, all vehicles are normally understeering vehicles, thus the front axle tends to saturate before the rear axle does. If the yaw moment M_z has the same sign as the yaw rate, which is denoted as "destabilising yaw moment" (for example, if a_y is positive, i.e. the vehicle turns left, and M_z is positive), i.e. counterclockwise, then according to 31 and 32 the front axle lateral force will be less than for the baseline vehicle (for which $M_z = 0$), while the rear axle will experience a larger force. This way it is possible to exploit more of the rear axle force availability, delaying the saturation of the front axle. Of course, M_z should not be excessive. Note that the effect of the combined (longitudinal-lateral) interaction should also be considered, since M_z is obtained through longitudinal forces.

The reference yaw rate, r_{ref}, can be obtained as an offline look-up table based on the following procedure:

- for given values of a_y, a_x, μ and V, calculate $\delta_{sw,dyn}$ by inverting 28, i.e.

$$\delta_{sw,dyn} = \begin{cases} K_{us} a_y & \text{if } a_y \le a_y^* \\ K_{us} a_y - K_{us}(a_{y,MAX} - a_y^*) \ln \frac{(a_{y,MAX} - a_y)}{(a_{y,MAX} - a_y^*)} & \text{if } a_y > a_y^* \end{cases} \tag{33}$$

- compute $\delta_{sw,kin}$ based on l, $R \approx V^2/a_y$ and the steering map of the vehicle
- compute $\delta_{sw} = \delta_{sw,kin} + \delta_{sw,dyn}$
- associate the above values of δ_{sw}, V, a_x to the steady-state relationship $r_{ref} = a_y/V$

Finally, the obtained dataset is inverted so as to provide the reference yaw rate as a function of measurable parameters, i.e. steering wheel angle, vehicle speed, longitudinal acceleration. An example is shown in Fig. 5. In practical applications, a first order lag is applied, as per 27.

The idea of designing the whole vehicle cornering response can be further extended to the design of not just one, but multiple understeer characteristics, denoted

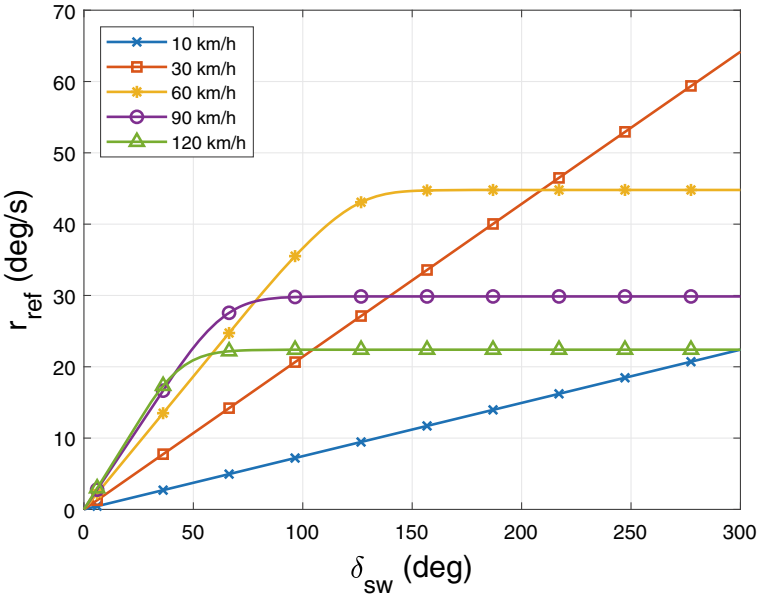

Fig. 5 Example of the reference yaw rate map as a function of the steering wheel angle for different values of vehicle speed, $a_x = 0$ (from Mangia et al., 2021)

as driving modes (De Novellis et al., 2015a). The driver may select a specific driving mode to adapt the vehicle behaviour according to specific driving conditions and/or driver needs or preferences, e.g. improving the fun-to-drive, adapting to low friction conditions, etc.

3.3 Concurrent Yaw Rate and Sideslip Angle Control

As discussed, the vehicle sideslip angle may also be taken into account, along with the vehicle yaw rate, in the reference generator. The main rationale for controlling the sideslip angle is related to vehicle stability:

- Yaw rate control normally requires a good estimate of the available friction coefficient (see 26 and 33). When the estimate is inaccurate,[5] r_{ref} may not be compatible with the available friction conditions, thus the vehicle may end up in safety-critical conditions, such as drifting or incipient loss of vehicle control, e.g. spin.
- The estimation of the available tyre-road friction coefficient is a very challenging research problem (Guo et al., 2018). However, the estimation of β is in general easier (Cheli et al., 2007; Chindamo et al., 2018).

[5] For instance, the yaw rate controller is designed for dry conditions, $\mu \approx 0.8 - 1$, but the road is wet. Or, even in dry conditions, μ happens to be overestimated.

- β is rather small in standard driving conditions, and it tends to assume relatively large values in safety-critical conditions. Hence, ensuring that β is limited through sideslip angle control is an effective way for enhancing vehicle stability.

Before describing some of the available solutions, an important concept should be pointed out and explained in detail. While it would be desirable to independently control both yaw rate and sideslip angle with a suitable yaw moment, actually that is not possible. The single-track vehicle model presented earlier (Eqs. 29, 30, 9, 10, 5, 6) can be rewritten, using $a_y = \dot{v} + ur \approx \dot{\beta}u + ur \approx \dot{\beta}V + Vr$, in the following state-space representation with state $x = \left[\beta\ r\right]^T$:

$$\dot{x} = Ax + B_i M_z + B_d \delta \tag{34}$$

where the dynamic matrix is

$$A = \begin{bmatrix} \dfrac{Y_\beta}{mV} & \dfrac{Y_r}{mV} - 1 \\ \dfrac{N_\beta}{J_z} & \dfrac{N_r}{J_z} \end{bmatrix} \tag{35}$$

the input matrix is

$$B_i = \begin{bmatrix} 0 \\ \dfrac{1}{J_z} \end{bmatrix} \tag{36}$$

the disturbance input matrix is

$$B_d = \begin{bmatrix} \dfrac{C_1}{mV} \\ \dfrac{C_1 a_1}{J_z} \end{bmatrix} \tag{37}$$

and the stability derivatives Y_β, Y_r, N_β and N_r are (Genta, 1997):

$$\begin{aligned} Y_\beta &= -\left(C_1 + C_2\right) \\ Y_r &= -\frac{\left(a_1 C_1 - a_2 C_2\right)}{V} \\ N_\beta &= -\left(a_1 C_1 - a_2 C_2\right) \\ N_r &= -\frac{\left(a_1^2 C_1 + a_2^2 C_2\right)}{V} \end{aligned} \tag{38}$$

From a control perspective, in 34 the yaw moment is the only input, while there is no control on the steering angle which is managed by the driver, so δ is for-

mally a disturbance. The system can be shown to be controllable[6]—more precisely, state-controllable. However, as discussed in Skogestad and Postlethwaite (2007), this property should better be denoted as "pointwise controllability" in the sense that although the system can possibly reach any desired configuration $[\beta_{ref} \quad r_{ref}]^T$, there is no guarantee that the system can hold such state values for a certain amount of time (from a very small amount of time to potentially ∞). To be able to control β and r independently, the system needs to be "functionally controllable" (Skogestad & Postlethwaite, 2007) which here reduces to requiring at least two control inputs. This point is also raised by Kaiser (2015) stating that, to control both yaw rate and sideslip angle, the yaw moment is not sufficient on its own and an additional control variable is needed, such as an active steering system.

With this in mind, many authors have proposed interesting techniques to design M_z by appropriately mediating between the two control targets while guaranteeing safety and stability for the vehicle. A standard approach is to define a reference sideslip angle, β_{ref}, and integrate it together with the reference yaw rate in the high level controller, as discussed in Sect. 4.

Different ways have been proposed to define β_{ref}. For instance, Siampis et al. (2016) choose β_{ref} as the sideslip angle obtained by a single-track model in steady-state conditions:

$$\beta_{ref} = \frac{C_2 l a_2 - a_1 m V^2}{C_2 l (l + K_{us} V^2)} \delta \tag{39}$$

which can be obtained from the equilibrium equations 11 and 12 by inserting 9, 10, 5, 6, assuming $\dot{r} = \dot{v} = 0$, then solving one of the equilibrium equations for r and substituting into the other equilibrium equation, and finally solving for $\beta(\delta)$. Note that the dependency on C_1 is embedded in K_{us}. An explicit version, without the use of K_{us}, is presented in Rajamani (2011).

As discussed above, the main rationale for controlling β is to ensure it does not exceed some safety-critical threshold, to ensure vehicle stability. For this reason, some authors simply choose $\beta_{ref} = 0$, however that does not necessarily ensure a maximum safety margin: β is the sideslip angle at the vehicle centre of mass, where even in case of slip-free conditions there is a non-zero kinematic contribution $\beta_{kin} \approx \frac{a_2}{l} \delta$ (Lenzo et al., 2017b).

On the same wavelength—i.e., bounding β—is the β_{ref} formula proposed in Vignati et al. (2016), which bounds the sideslip angle within $\pm\beta_{th}$, where β_{th} is a threshold representing the maximum acceptable magnitude of β:

$$\beta_{ref} = \beta_{th} \tanh\left(\frac{\beta}{\beta_{th}}\right) \tag{40}$$

where β is the current value of sideslip angle.

[6] Unless $mV^2 + C_1 a_1 - C_2 a_2 = 0$.

Since, as discussed, controlling r and β at the same time with M_z is challenging, it is clear that imposing both references at the same time implies that, in general, neither of them will be followed exactly—the relative priority may be defined, e.g., by appropriately weighting a yaw rate-based yaw moment contribution and a sideslip angle-based yaw moment contribution, or through the elements of matrix Q in the LQR cost function 56. Hence, even in standard driving conditions with small β, the yaw rate tracking performance (handling requirement) would be compromised without significant stability benefits. It would then seem reasonable to develop a control that accounts for β only when its magnitude is of concern, i.e., beyond a certain threshold. As a result, the handling requirement would not be sacrificed unless stability becomes a priority. This idea may be exploited in two different ways, as detailed below.

In Tota et al. (2018),

$$\beta_{ref} = \begin{cases} \beta & \text{if } |\beta| < \beta_{th} \\ \beta_{th}\text{sgn}(\beta) & \text{if } |\beta| \geq \beta_{th} \end{cases} \tag{41}$$

The interpretation of 41 is that, when the value of β is not of concern, the reference sideslip angle is imposed as the same as the current sideslip angle, i.e. no sideslip-related control action is required because there is purposely no difference between β_{ref} and β. So, the yaw moment is only used to track r_{ref}. Another relevant aspect of this approach is that when $\beta_{ref} \neq \beta$, i.e. an intervention on the sideslip angle is required, the reference yaw rate is corrected with a contribution proportional to the yaw rate variation provoked by the sideslip-related yaw moment contribution.[7]

The solution presented in Lenzo et al. (2021), instead, does not need to define a β_{ref}, yet it proposes a correction of the reference yaw rate based on the actual value of sideslip angle:

$$r_{ref} = r_h - F(r_h - r_s) \tag{42}$$

where r_h is the reference yaw rate calculated on the basis on handling requirements, e.g. through 25 or the procedure described in Sect. 3.2. The stability yaw rate, r_s, represents an achievable yaw rate in the current tyre-road friction conditions:

$$r_s = \begin{cases} r_h & \text{if } |r_h| < (\frac{a_y - \text{sgn}(a_y)\Delta a_y}{V}) \\ |\frac{a_y - \text{sgn}(a_y)\Delta a_y}{V}|\text{sgn}(r_h) & \text{if } |r_h| \geq (\frac{a_y - \text{sgn}(a_y)\Delta a_y}{V}) \end{cases} \tag{43}$$

The factor F is defined as:

$$F = \begin{cases} 0 & \text{if } |\beta| < \beta_{act} \\ k_1 \frac{|\beta| - \beta_{act}}{\beta_{th} - \beta_{act}} & \text{if } \beta_{act} \leq |\beta| \leq \beta_{th} \\ k_2 & \text{if } |\beta| > \beta_{th} \end{cases} \tag{44}$$

[7] See Table 1 in Tota et al. (2018).

and k_1, k_2 and Δa_y are positive tuning parameters. The parameters β_{act} and β_{th} represent respectively an activation threshold and, again, an upper threshold. If $|\beta| < \beta_{act}$, there is no sideslip-based correction in 42.

The key aspect of this solution is that the reference generator produces a single output, r_{ref}, and it accounts for β-related requirements, too. This benefits the design of the high level controller, which is not required to mediate between conflicting targets. Although a mediation between yaw rate and sideslip angle requirements is inevitable (because the system is functionally uncontrollable), here such mediation is achieved at the level of the reference generator, allowing for a more "physical" design approach. It is also worth to mention that a similar control principle was adopted in Zanchetta et al. (2019) for the concurrent control of yaw rate and hitch angle for an articulated vehicle (a car towing a trailer).

Finally, Gasmi et al. (2019) present an interesting review on how to possibly choose β_{th}—some authors propose a formula depending on μ (Rajamani, 2011), others propose a formula depending on V (Kiencke & Nielsen, 2000). A sensitivity analysis on β_{act} and β_{th} is also provided in Lenzo et al. (2021).

4 High Level Controller: T_{tot}, M_z

This section briefly describes methods to determine T_{tot}, then it extensively discusses how to elaborate M_z. The final part of this section presents experimental results obtained on a vehicle prototype within the European Project iCOMPOSE (Lenzo et al., 2019b) and further practical remarks.

A general aspect relevant for both T_{tot} and M_z is the understanding of feedforward and feedback controllers. Given a reference value for the generic variable of interest (e.g. the vehicle speed in case of T_{tot}, or the yaw rate in case of M_z):

- A *feedforward control action* is calculated based on a mathematical model of the system to be controlled, regardless of the actual value of the variable of interest.
- A *feedback control action* is calculated based on the error, i.e. the difference between reference value and actual value of the variable of interest.

Often a combination of feedforward and feedback actions is used, to blend their benefits. The reason is that the feedforward contribution helps to provide a fast response of the system (the control action is generated straightaway, hence no need to wait for the feedback action to build up[8]), while the feedback contribution allows to compensate for unmodeled effects and disturbances— both practically unavoidable—thus ensuring a precise tracking action. While feedforward controllers are rarely used alone, it is not uncommon to use feedback controllers only. For a much more complete discussion on this topic, the interested reader is referred to Isermann (2012) and De Novellis et al. (2015b).

[8] For instance, e.g., Manning and Crolla (2007) suggest that the feedforward contribution "tends to reduce the time lag between steer angle input and vehicle reaction".

4.1 Calculation of T_{tot}

Traditionally, T_{tot} is calculated (Fig. 2) based on accelerator and brake pedal positions (driver input) and vehicle speed (vehicle state). First, the desired total traction/braking force for the vehicle, F_{tot}, can be computed. Then, the desired total torque can be calculated based on F_{tot}, the wheel dynamics (depending on the wheel angular acceleration and on the wheel moment of inertia) and the wheel radius (which in general is not constant, Vantsevich et al., 2005, 2017). In a simplified scenario, $T_{tot} = F_{tot}R_w$, where the wheel dynamics is neglected and R_w is the average wheel radius, assumed constant.

To compute F_{tot}, the accelerator and brake pedal positions can be interpreted to define a value of desired acceleration, a_{des}. Then, an option is to calculate F_{tot} based on a simplified vehicle equilibrium equation:

$$F_{tot} - F_r = ma_{des} \tag{45}$$

which essentially states that F_{tot} needs to generate a_{des} while: (i) overcoming the resistance contributions, F_r, during traction; (ii) accounting for the favourable action of F_r, during braking. F_r includes contributions such as aerodynamic drag and rolling resistance, which can be modelled rather easily with reasonable approximation (Genta, 1997).

Alternatively, a more precise characterisation of F_r can be obtained with coast down tests (Preda et al., 2010; White & Korst, 1972), and it can be embedded in a generic drivability map that produces F_{tot} based on vehicle speed and accelerator/brake pedal positions, as in Lenzo et al. (2017b).

Clearly, both 45 and the drivability map are feedforward approaches. However in some cases, e.g. when performing standardised manoeuvres or simply during highway driving, reaching and maintaining a certain speed may be necessary. That can be easily achieved through a feedback approach, e.g. a PID (Proportional-Integral-Derivative) controller based on the difference between reference and current value of vehicle speed.[9]

4.2 Calculation of M_z

To calculate M_z it is customary to use either a feedback controller of a combination of a feedforward and a feedback controller. To understand the practical implications of each contribution, it is useful to look at the equilibrium equations of a classic double-track vehicle model (Fig. 6):

$$ma_x = F_{x_{11}} \cos\delta_{11} + F_{x_{12}} \cos\delta_{12} + F_{x_{21}} + F_{x_{22}} - F_{y_{11}} \sin\delta_{11} - F_{y_{12}} \sin\delta_{12} - F_r \tag{46}$$

[9] In other words, a simple "cruise control" logic.

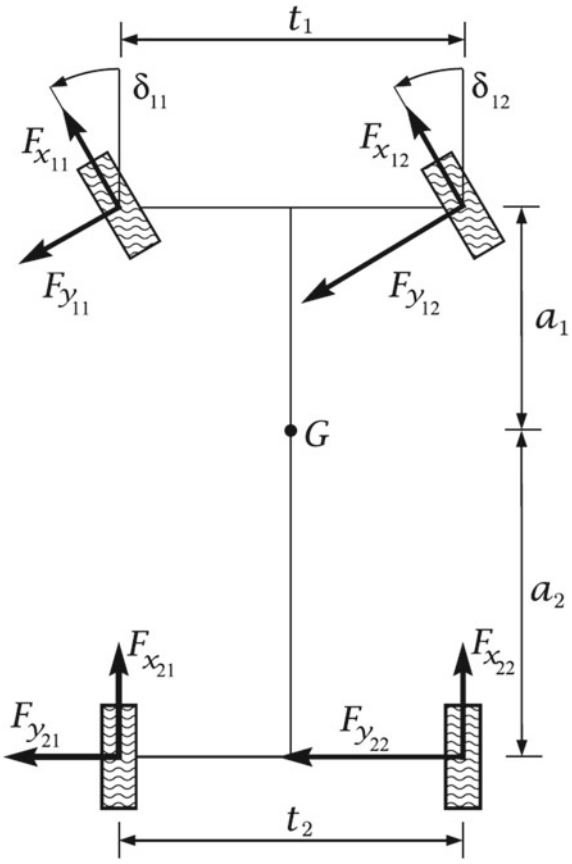

Fig. 6 Double track vehicle model (adapted from Guiggiani, 2018)

$$ma_y = F_{y_{11}} \cos\delta_{11} + F_{y_{12}} \cos\delta_{12} + F_{y_{21}} + F_{y_{22}} + F_{x_{11}} \sin\delta_{11} + F_{x_{12}} \sin\delta_{12} \quad (47)$$

$$\begin{aligned} J_z\dot{r} = {} & (F_{y_{11}} \cos\delta_{11} + F_{y_{12}} \cos\delta_{12} + F_{x_{11}} \sin\delta_{11} + F_{x_{12}} \sin\delta_{12})a_1 + \\ & -(F_{y_{21}} + F_{y_{22}})a_2 + (F_{x_{12}} \cos\delta_{12} - F_{x_{11}} \cos\delta_{11})\frac{t_1}{2} + \\ & +(F_{x_{22}} - F_{x_{21}})\frac{t_2}{2} + (F_{y_{11}} \sin\delta_{11} - F_{y_{12}} \sin\delta_{12})\frac{t_1}{2} \end{aligned} \quad (48)$$

where $F_{x_{ij}}$ and $F_{y_{ij}}$ are, respectively, the longitudinal and lateral tyre-road forces for wheel ij, t_i the vehicle tracks, δ_{1j} the wheel steer angles, $i = 1, 2$ respectively for front and rear axle, and $j = 1, 2$ respectively for left and right side.

The yaw equilibrium equation, 48, can be rewritten as:

$$J_z\dot{r} = N_f + N_y + N_d \tag{49}$$

where:

$$N_f = F_{x_{11}} \sin\delta_{11} a_1 + F_{x_{12}} \sin\delta_{12} a_1 \tag{50}$$

$$N_y = (F_{y_{11}} \cos\delta_{11} + F_{y_{12}} \cos\delta_{12}) a_1 - (F_{y_{21}} + F_{y_{22}}) a_2 + (F_{y_{11}} \sin\delta_{11} - F_{y_{12}} \sin\delta_{12}) \frac{t_1}{2} \tag{51}$$

$$N_d = (F_{x_{12}} \cos\delta_{12} - F_{x_{11}} \cos\delta_{11}) \frac{t_1}{2} + (F_{x_{22}} - F_{x_{21}}) \frac{t_2}{2} \tag{52}$$

Based on the idea of torque vectoring presented at the beginning of this Chapter, the variables that can actually be controlled to generate a yaw moment are the longitudinal forces, $F_{x_{ij}}$. So, $M_z = N_f + N_d$, where $N_d \gg N_f$ because in normal driving conditions $\delta_{ij} \ll 1$.

On the other hand, it is quite difficult to model the behaviour of N_y because there is no direct control on the lateral forces, $F_{y_{ij}}$. These depend on the tyre behaviour, that is challenging to characterise accurately, especially in real time (Acosta & Kanarachos, 2018; Guo et al., 2018). Furthermore, it should be noted that M_z itself influences the lateral forces (e.g. see 31, 32) and, as a consequence, the vertical loads (see paragraph 2.4 in Frendo et al. (2007)) which in turn affect the lateral forces. These aspects further justify why a feedforward control alone is not a suggested option for direct yaw moment control, yet it should be used together with a feedback contribution.

With that in mind, it is still of interest to derive an expression for a feedforward yaw moment, $M_{z,FF}$. For simplicity, here this is done for a single-track vehicle model with linear tyres.[10] Starting from the equilibrium equations 29 and 30, considering $\beta \ll 1$ and quasi-steady-state conditions ($\dot{\beta} = \dot{r} = 0$, but it might be $\dot{V} \neq 0$):

$$F_{y_1} + F_{y_2} = ma_y = m(\dot{v} + ur) \approx m(\dot{V}\beta + V\dot{\beta} + Vr) = m(\dot{V}\beta + Vr) \tag{53}$$

$$F_{y_1} a_1 - F_{y_2} a_2 + M_{z,FF} = J_z\dot{r} = 0 \tag{54}$$

By using the congruence equations 1 and 2, as well as the constitutive equations 9 and 10, setting $r = r_{ref}$ and rearranging for $M_{z,FF}$:

[10] In principle the double-track model above could also be used, with potentially any tyre model—however in case of strong nonlinearities and/or if the tyre model accounts for combined interactions, for computational reasons it would be more appropriate to derive a $M_{z,FF}$ map, as in De Novellis et al. (2013).

$$M_{z,FF} = -\frac{(-C_1a_1 + C_2a_2)(C_1\delta V - r_{ref}(C_1a_1 - C_2a_2 + mV^2))}{V(m\dot{V} + C_1 + C_2)} + \\ + \frac{C_1(a_1^2 + a_2^2)}{V} r_{ref} - C_1a_1\delta \tag{55}$$

It is worth to remark that this value of $M_{z,FF}$ would bring the reference yaw rate to r_{ref} (with no need of feedback controller) if, ideally, the system behaves exactly according to the equations used above. Finally, because it was obtained in quasi-steady-state conditions, the above expression for $M_{z,FF}$ might provoke undesired yaw rate oscillations and overshoots in extreme transients. Such issue can be addressed by adding a dynamic feedforward contribution that modifies the transient response of the system, which can be designed in the Laplace domain as shown in De Novellis et al. (2015b).

For the feedback contribution, a widely used approach is the implementation of a PID controller (Aastrom & Murray, 2010) based on the error between reference and actual value of the controlled variable, e.g. the yaw rate. Practically, when an integral contribution is present, suitable reset conditions—e.g. depending on a_y (or the error) being within a predetermined threshold or not—and an anti-windup correction should be included (De Novellis et al., 2015b). The PID parameters may be tuned in many ways, including the Ziegler-Nichols method, the Linear Quadratic Regulator (LQR) (He et al., 2000) etc. In the LQR case, the idea is to minimise the following performance index:

$$J = \int_0^\infty \left(x^T Q x + M_z R M_z\right) dt \tag{56}$$

which needs a linear model of the system rearranged in the form

$$\dot{x} = Ax + B_i M_z + U \tag{57}$$

where x is a vector containing the error and its derivative/integral as appropriate (e.g., the error and its integral if a PI scheme is used), A is the dynamic matrix, B_i is the input matrix, and U is everything else (e.g. steering angle contribution as in 34, modelled disturbances). For example, Vignati et al. (2016) use a single-track vehicle model with linear tyres and a Proportional-only controller for yaw rate and sideslip angle, for which $x = [\beta_{ref} - \beta \quad r_{ref} - r]^T$ applies. The matrices $Q \geq 0$ and $R > 0$ penalise excessive error and excessive control action, respectively. The optimal control action, M_z^{opt}, can be computed as[11]:

$$M_z^{opt} = -R^{-1} B_i^T P x \tag{58}$$

[11] The interested reader might find interesting to know how to obtain this result from, e.g., Stanford-University (2020).

where $P = P^T \geq 0$ is the solution of the following Algebraic Riccati Equation (ARE):[12,13]

$$A^T P + PA - PB_i R^{-1} B_i^T P + Q = 0 \tag{59}$$

Further interesting approaches for the feedback controller are H-∞ control (Lu et al., 2016), Sliding Mode Control (SMC) and its variants such as Second Order Sliding Mode (SOSM), Integral Sliding Mode (ISMC) (Goggia et al., 2015; Chen et al., 2018), explicit or implicit Model Predictive Control (MPC) (Zhou & Liu, 2009; Guo et al., 2020). In Parra et al. (2018) M_z is calculated through a fuzzy logic approach based on sideslip angle error, yaw rate error and yaw rate error derivative. A comparison among four feedback control techniques, including PID and SOSM, is presented in De Novellis et al. (2014c).

It is also possible to combine multiple feedback action schemes. For instance Tota et al. (2018) combine a PI controller with an ISMC controller. The PI controller gains are obtained through a LQR according to Eqs. 56 and 57, with $x = [\beta_{ref} - \beta \quad r_{ref} - r \quad \eta]^T = [e_\beta \quad e_r \quad \eta]^T$, and $\dot{\eta} = e_r$. The ISMC (based on a suitable sliding variable[14] accounting for both e_β and e_r) is used to estimate the system perturbation, so the nominal controller (PI) is continuously enhanced by the ISMC perturbation compensator.

4.3 Experimental Results and Further Remarks

This section present a selection of relevant experimental results obtained within the European Project iCOMPOSE (Lenzo et al., 2019b). The vehicle demonstrator was a Range Rover Evoque prototype equipped with four identical on-board electric powertrains (Figs. 7 and 8).

Based on the approach described in Sect. 3.2, Fig. 9 shows:

- The experimental cornering response of the vehicle obtained via skid-pad tests with the baseline configuration (no yaw moment) and with the controlled vehicle using a driving mode denoted as "Sport mode"—because it implies increased steering responsiveness (less understeer gradient than the baseline configuration). As per design, the region of linear vehicle operation is extended and the maximum lateral acceleration is increased.
- The yaw rate measured during step steer tests (100 km/h, 100°) for the baseline vehicle and the "Sport mode" controlled vehicle, highlighting that even if the

[12] Note that this is not a Differential Riccati Equation (DRE) because of the infinite horizon used in 56 (otherwise the right-hand-side of this equation would be $-\dot{P}$ instead of 0).

[13] Because the single-track vehicle model assumes constant vehicle speed, a gain scheduling approach is often implemented.

[14] The interested reader is also referred to Utkin and Shi (1996), Utkin et al. (2017).

controller is designed in quasi-steady-state conditions,[15] it brings benefits in transients, too. Specifically, it is possible to observe a considerable reduction of the yaw rate oscillations and of the settling time.

Figure 10 depicts the measured sideslip angle during step steer manoeuvres in which the vehicle implemented the concurrent yaw rate and sideslip controller from Tota et al. (2018), based on PI+ISMC. Here, the sideslip thresholds are intentionally set to large values so as to achieve a controlled drift condition with the desired value of sideslip angle. Similar experimental results are discussed in Lenzo et al. (2021).

Before presenting results of the concurrent yaw rate and sideslip angle control (through Eqs. 42, 43, 44), it is interesting to note that the whole discussion presented in Sect. 3.3 implicitly assumed that the controller uses the classically defined sideslip angle, i.e. the angle between the vehicle longitudinal axis and the velocity vector at the centre of mass (CM) of the vehicle (this was also used in Sect. 3.1: $\beta = \arctan v/u$). Despite this is very common in the literature, it is also natural to wonder what the effect of a difference reference point would be on the controller. This was studied in Lenzo et al. (2017b), which tested the controller using, in 44, values of sideslip angle at different points of the vehicle specifically the front axle, the centre of mass and the rear axle. The PI+ISMC controller discussed above was used as high level controller.

The resulting sideslip angle at the centre of mass for a slalom manoeuvre on a slippery road is shown in Fig. 11, while Fig. 12 shows two relevant frames captured at the test facility. While the baseline vehicle (no yaw moment) produces large values

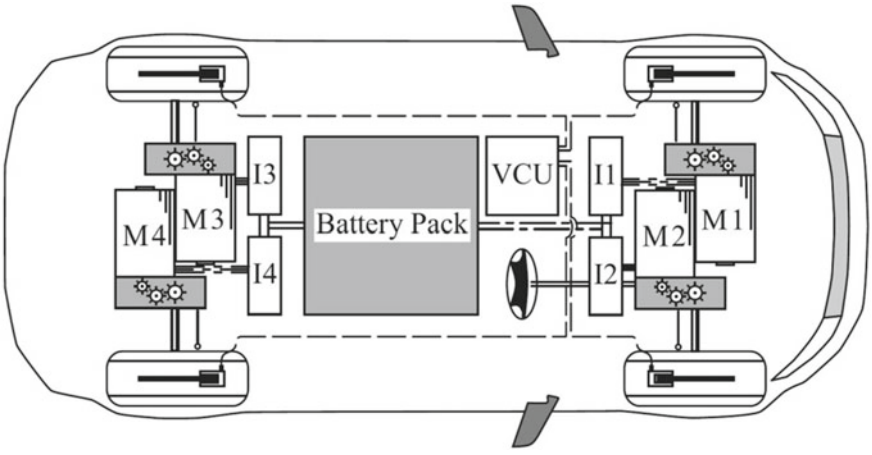

Fig. 7 Schematic of the architecture of the Range Rover Evoque demonstrator. M1-M4 = switched reluctance motors; I1-I4 = inverters; VCU = vehicle control unit (reproduced from Lenzo et al., 2019b)

[15] The reference yaw rate is designed based on the steady-state relationship $r_{ref} = a_y/V$, but in general $a_x \neq 0$ is also allowed.

Fig. 8 The Range Rover Evoque during an obstacle avoidance manoeuvre (ISO 3888-2)

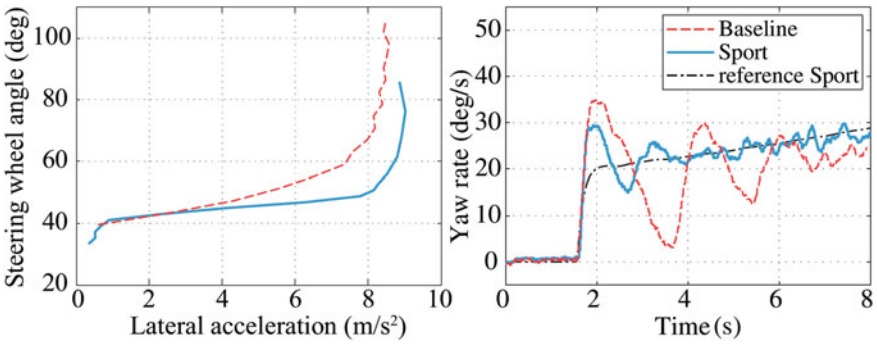

Fig. 9 Results of the design of the understeer characteristics: (left) experimental cornering response; (right) yaw rate response (and reference value) during step steer tests (reproduced from Gruber et al., 2016)

of β, the controlled vehicle based only on handling requirements for standard road conditions is even worse, eventually spinning shortly after 8 s (Fig. 11). On the other hand, when the sideslip angle is accounted for in the definition of the reference yaw rate, the controller provides a significantly smoother, more consistent and safer vehicle behaviour.[16] Interestingly, Fig. 11 shows that when the sideslip angle at the

[16] It should also be noted that compared to a conventional ESC, the torque vectoring controller interventions can be seamlessly and continuously generated, without necessarily decreasing the vehicle speed.

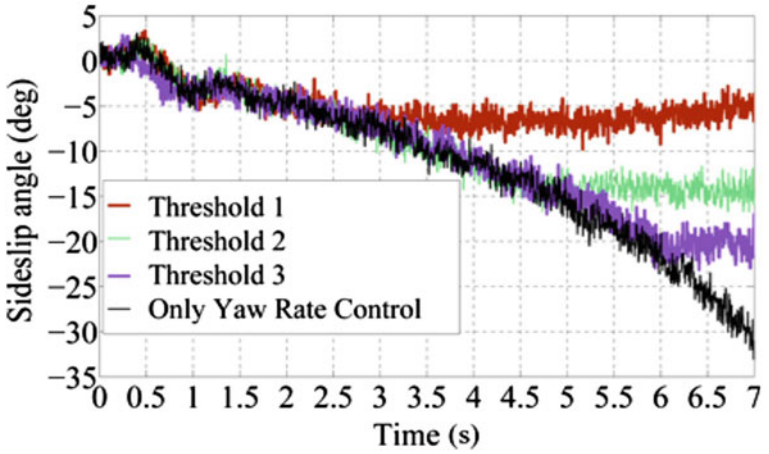

Fig. 10 Vehicle sideslip angle control during step steer tests (reproduced from Tota et al., 2018)

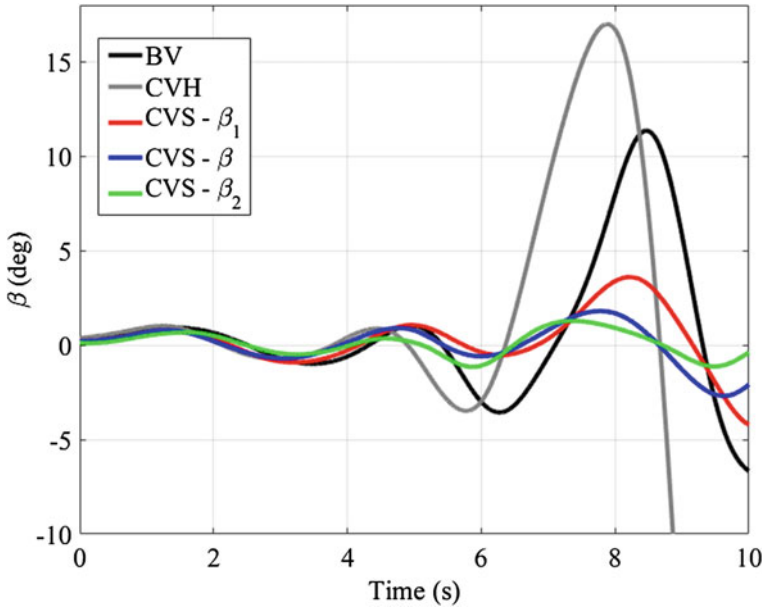

Fig. 11 Time history of the vehicle sideslip angle during a slalom on a slippery road, for different vehicle configurations: Baseline vehicle (BV), controlled vehicle solely based on the handling yaw rate (CVH), controlled vehicle with concurrent yaw rate and sideslip angle control, for three positions of the sideslip angle used in the controller formulation (CVS) (reproduced from Lenzo et al., 2017b)

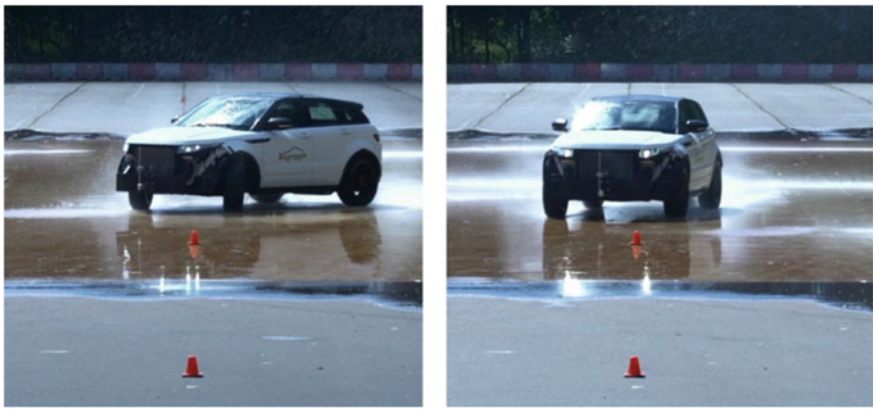

Fig. 12 A slalom test on a slippery road: (left) without controller, the driver needs to countersteer to keep the vehicle on track; (right) with controller, providing a much smoother behaviour (reproduced from Lenzo et al., 2017b)

rear axle, β_2, is used in 44, the sideslip angle remains within a tighter range than when using either β or β_1.[17] The reason of this effect is discussed hereinafter.

The sideslip angle at a generic point P, β_P, can be defined as the angle between the vehicle longitudinal axis and the velocity vector at P or, equivalently, the arc tangent of the ratio between lateral and longitudinal components of the velocity of P. These components can be easily computed through fundamental rigid body kinematic formulas such as Rivals theorem, as shown below. Figure 13 shows a schematic including velocities (V) and sideslip angles (β) at the vehicle front axle, centre of mass (CM), rear axle and a generic point P (note that in the x-y reference system chosen, x_P is positive and y_P is negative). Once known u and v, hence the sideslip angle at the centre of mass, $\beta = \arctan v/u$,[18] then the sideslip angle at the generic point P is:

$$\beta_P = \arctan \frac{v + r x_P}{u - r y_P} \tag{60}$$

which reduces to 3 or 4 when P coincides respectively with the centre of the front axle or the rear axle. A further relevant point is that in general there are two contributions to sideslip angle: a kinematic contribution and a dynamic contribution. For the generic point P, it is

$$\beta_P = \beta_{P,kin} + \beta_{P,dyn} \tag{61}$$

[17] Figure 11 plots β, but the same trend was found also for the other locations, as discussed in Lenzo et al. (2017b).

[18] In iCOMPOSE a dedicated sideslip angle sensor was used, to ensure a reliable measurement of u and v in any condition, so as to be able to fully focus on the design of the controllers.

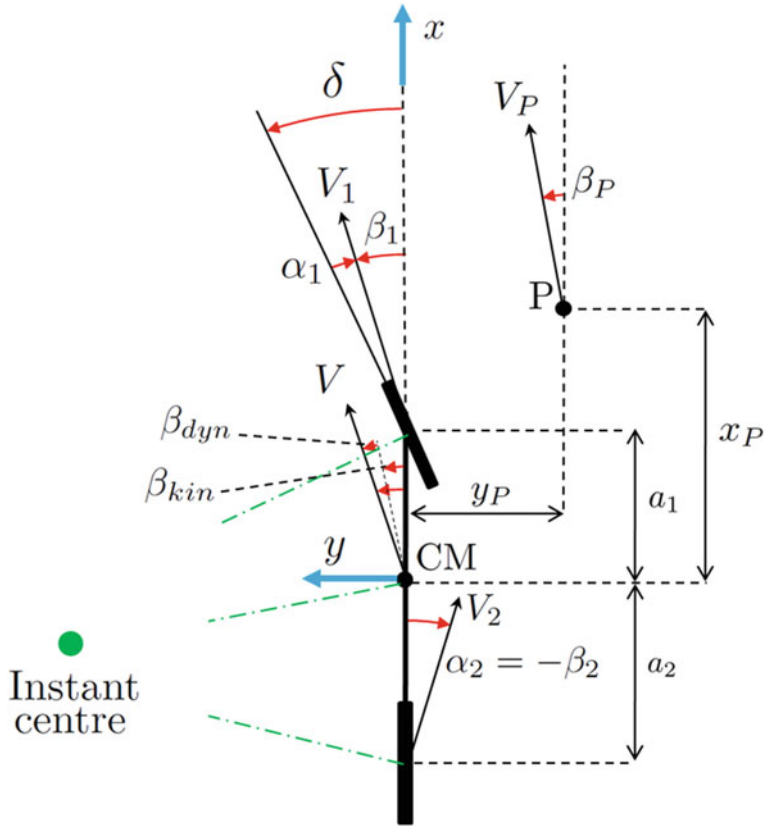

Fig. 13 Vehicle schematic showing relevant quantities at: front axle, centre of mass (CM), rear axle, generic point P

The kinematic contribution, $\beta_{P,kin}$, is by definition related to the vehicle kinematics, in particular to the steering angle and some geometrical quantities. The dynamic contribution, $\beta_{P,dyn}$, is instead related to slip angles. The kinematic and dynamic sideslip contribution at the centre of mass, respectively β_{kin} and β_{dyn}, are shown in Fig. 13. From a control design point of view, it would not make sense to try and correct a kinematic contribution because this is, by definition, an intrinsic property of the system.[19] The ideal target of the control action is the dynamic contribution only, which is consistent with the idea of limiting tyre slips. Provided that there is no rear steering capability, the kinematic sideslip angle contributions at front axle, centre of mass and rear axle can be approximated respectively as δ, $\delta a_2/l$, 0.[20] As a

[19] Another example would be a parking manoeuvre, which entails high steering angles, hence high kinematic sideslip angles, but low tyre slips, hence small dynamic sideslip angles.

[20] That is, the wheel steer angle divided by the vehicle wheelbase and multiplied by the distance between the rear axle and the point of interest.

result, $\beta_2 = \beta_{2,dyn}$, implying that controlling β_2 in 44 implies that only the dynamic sideslip angle contribution is corrected by the controller. This is also consistent with the fact that the rear axle is responsible for stability in cornering. This explains the results of Fig. 11.

Another important aspect of experimental testing (and simulation) is the objective assessment of performance of the developed controllers. To do so, it is customary to adopt appropriate performance indices. In general these can be defined depending on the specific application. Here, some of the most common performance indices are reported:

- the root mean square error (RMSE) of the magnitude of the yaw rate error, $RMSE_r$, which assesses the yaw rate tracking performance:

$$RMSE_r = \sqrt{\frac{1}{t_f - t_i}\int_{t_i}^{t_f} (r_{ref}(t) - r(t))^2 \mathrm{d}t} \tag{62}$$

  where t_i and t_f are, respectively, the initial and final time of the relevant part of the recorded dataset (e.g. initial and final time of a specific manoeuvre);
- the root mean square error of the magnitude of the sideslip angle error, $RMSE_\beta$, which assesses the sideslip angle tracking performance[21]:

$$RMSE_\beta = \sqrt{\frac{1}{t_f - t_i}\int_{t_i}^{t_f} (\beta_{ref}(t) - \beta(t))^2 \mathrm{d}t} \tag{63}$$

- the normalised integral of the magnitude of the control action, $IACA$, which assesses the amount of yaw moment effort:

$$IACA = \frac{1}{t_f - t_i}\int_{t_i}^{t_f} |M_z(t)| \mathrm{d}t \tag{64}$$

Further performance indices for the concurrent control of yaw rate and sideslip angle are discussed in Lenzo et al. (2017b).

5 Low Level Controller: T_{ij}

This section elaborates the mathematical relationships between the outputs of the high level controller (T_{tot} and M_z) and T_{ij}. Then, specific criteria on how to achieve an optimal distribution of the wheel torque are discussed. The final part of this section presents experimental results, obtained on the same vehicle prototype seen in Sect. 4.3, and further practical remarks.

[21] Obviously this index makes sense only if β_{ref} is defined. As discussed, concurrent yaw rate and sideslip control is possible even without defining β_{ref}, by integrating the sideslip angle in the reference yaw rate formulation, as shown in 42.

5.1 Relationships Among T_{tot}, M_z and T_{ij}

The role of the low level controller is to determine T_{ij} that satisfy the following general expressions, which can be obtained through a basic free body diagram of the vehicle[22] (Fig. 6):

$$\sum_{i,j} F_{ij} \cos \delta_{ij} = F_{tot} \tag{65}$$

$$\sum_{i,j} (-1)^j F_{x_{ij}} \frac{t_i}{2} \cos \delta_{ij} - \sum_{i,j} (-1)^i F_{x_{ij}} \frac{a_i}{2} \sin \delta_{ij} = M_z \tag{66}$$

By neglecting the wheel dynamics and assuming that the wheel radius is approximately the same for all wheels, $F_{x_{ij}} = T_{ij}/R_w$, 65 and 66 reduce to:

$$\sum_{i,j} T_{ij} \cos \delta_{ij} = T_{tot} \tag{67}$$

$$\sum_{i,j} (-1)^j \frac{T_{ij}}{R_w} \frac{t_i}{2} \cos \delta_{ij} - \sum_{i,j} (-1)^i \frac{T_{ij}}{R_w} \frac{a_i}{2} \sin \delta_{ij} = M_z \tag{68}$$

Finally, because in normal driving conditions $\delta_{ij} \ll 1$, 67 and 68 become:

$$\sum_{i,j} T_{ij} = T_{tot} \tag{69}$$

$$\sum_{i,j} (-1)^j \frac{T_{ij}}{R_w} \frac{t_i}{2} = M_z \tag{70}$$

For a vehicle with two motors (e.g. front left and front right), this is a system of two equations and two unknows, which is completely determined. If the vehicle features more than two actuators, there are more unknowns than equations, meaning additional DOF can be conveniently exploited. For a typical vehicle configuration with four electric motors, 69 and 70 become[23]

$$T_{11} + T_{12} + T_{21} + T_{22} = T_{tot} \tag{71}$$

$$-\left(\frac{T_{11}}{R_w}\frac{t_1}{2} + \frac{T_{21}}{R_w}\frac{t_2}{2}\right) + \left(\frac{T_{12}}{R_w}\frac{t_1}{2} + \frac{T_{22}}{R_w}\frac{t_2}{2}\right) = M_z \tag{72}$$

[22] Note that lateral force contributions, $F_{y_{ij}}$ do not appear in these equations because they cannot be controlled, as extensively discussed in Sect. 4.2.

[23] Note that 68 is equivalent to $N_d + N_f = M_z$, where N_d and N_f are given in 52 and 50.

By introducing the reasonable assumption that front and rear track widths are the same, $t_1 = t_2 = t$, 72 can be rewritten as:

$$-(T_{11} + T_{21}) + (T_{12} + T_{22}) = M_z \frac{2R_w}{t} \tag{73}$$

where it is now possible to isolate the torque demand for each side of the vehicle: $T_L = T_{11} + T_{21}$ for the left side, $T_R = T_{12} + T_{22}$ for the right side. So, 71 and 73 can be rewritten as:

$$T_L + T_R = T_{tot} \tag{74}$$

$$-T_L + T_R = M_z \frac{2R_w}{t} \tag{75}$$

Solving 74 and 75 for T_L and T_R:

$$T_L = \frac{T_{tot}}{2} - \frac{M_z R_w}{t} = \frac{T_{tot}}{2} - \Delta T_{RL} \tag{76}$$

$$T_R = \frac{T_{tot}}{2} + \frac{M_z R_w}{t} = \frac{T_{tot}}{2} + \Delta T_{RL} \tag{77}$$

where the torque bias between right and left side is defined as

$$\Delta T_{RL} = \frac{-T_L + T_R}{2} = \frac{M_z R_w}{t} \tag{78}$$

As a result, the desired total torque and yaw moment demand at vehicle level are equivalent to two independent values of torque demand, one per each side of the vehicle (76 and 77). Since the overall torque demand for each side is determined, the two available DOF can simply be seen as torque distribution factors between front and rear motor, one per each side. Hence, the four wheel torque demands, T_{ij}, can be written in the form:

$$\begin{cases} T_{11} = \left(\frac{T_{tot}}{2} - \Delta T_{RL}\right)\sigma_L \\ T_{21} = \left(\frac{T_{tot}}{2} - \Delta T_{RL}\right)(1 - \sigma_L) \\ T_{12} = \left(\frac{T_{tot}}{2} + \Delta T_{RL}\right)\sigma_R \\ T_{22} = \left(\frac{T_{tot}}{2} + \Delta T_{RL}\right)(1 - \sigma_R) \end{cases} \tag{79}$$

where σ_L and σ_R are front-to-total torque ratios, respectively for left and right vehicle side.

Based on the independence of the vehicle sides, the following section will discuss how to optimally choose the front-to-total torque ratio, σ, for a generic vehicle side.

5.2 Computation of σ

In principle, any optimisation criterion may be used in the low level controller to determine σ. Typically, energy efficiency criteria are adopted. It is then important to appreciate what the sources of power loss are and how to handle them.

The study Pennycott et al. (2015) extensively discusses the main sources of power loss for electric vehicles. While power losses due to aerodynamic drag and rolling resistance are of significance, they depend on parameters such as the vehicle speed, so they cannot be influenced by σ. Power losses caused by drivetrains (electric motors, inverters, transmissions if present) and tyre slips, instead, are affected by wheel torque distribution.

The tyre slip power losses can be divided in longitudinal slip power losses and lateral slip power losses, and their expressions are respectively

$$P_{loss,x,ij} = F_{x_{ij}} v_{slip,x,ij} \tag{80}$$

and

$$P_{loss,y,ij} = F_{y_{ij}} v_{slip,y,ij} \tag{81}$$

where $v_{slip,x,ij}$ and $v_{slip,y,ij}$ are, respectively, the longitudinal and the lateral slip speed at wheel ij. Some studies choose to focus on the minimisation of tyre slip power losses by selecting σ based on the estimated vertical load on each wheel, with the idea to allocate higher torque demands where there is more vertical load, i.e. more availability of grip. In doing so, many authors assume a linear relationship between available grip and vertical load (Parra et al., 2018), that is only an approximation and may be inaccurate (Guiggiani, 2018). In any case, tyre slip power losses are often less significant than drivetrain power losses, unless the vehicle experiences high lateral accelerations (Pennycott et al., 2015). Other studies have shown that in some cases, depending on the type of electric motor installed, optimising slip losses might be slightly better than optimising drivetrain power losses (De Novellis et al., 2013, 2014b). However, relying on tyre slips may not actually be viable, because tyre slips are not directly measurable and their estimation is still challenging (Guo et al., 2018). This has motivated many studies on methods to minimise the power losses occurring in the drivetrains.

Drivetrain power losses have shown to be fairly well represented by third order polynomial functions of speed and torque demand (Lin & Xu, 2015; Mahmoudi et al., 2015; Lenzo et al., 2017a). Specifically Mahmoudi et al. (2015) propose:

$$P_{loss,ij}(T_{ij}, \omega_{ij}) = \sum_{m,n} k_{mn} \left(\frac{T_{ij}}{T_0}\right)^m \left(\frac{\omega_{ij}}{\omega_0}\right)^n P_0 \qquad m, n = 1, 2, 3 \tag{82}$$

where ω_{ij} is the angular speed of motor ij and T_0, ω_0 and P_0 are normalising factors. Instead, Lenzo et al. (2017a) interpolate the drivetrain power losses with a cubic polynomial function of the sole torque demand:

$$P_{loss,ij}(T_{ij}, V) = a_{ij}(V)T_{ij}^3 + b_{ij}(V)T_{ij}^2 + c_{ij}(V)T_{ij} + d_{ij}(V) \tag{83}$$

with the coefficients a_{ij}, b_{ij}, c_{ij} and d_{ij} depending on the vehicle speed, V. The physical interpretation of d_{ij} is that it represents losses independent of T_{ij}, such as those due to rolling resistance.

The contributions Dizqah et al. (2016), Lenzo et al. (2017a) propose fast parametric torque allocation strategies—denoted as control allocation (CA) strategies—based on the experimental assessment of the drivetrain power losses. Both studies make the hypothesis (verified experimentally) that $P_{loss,ij}$ is a strictly monotonically increasing function of T_{ij}, and that $P_{loss,ij}$ has an inflection point, i.e. a transition between a concave shape and a convex shape, for a positive value of T_{ij}. Applying these requirements to 83 implies $a_{ij}, c_{ij}, d_{ij} > 0$, $b_{ij} < 0$, and $b_{ij}^2 < 3a_{ij}c_{ij}$.[24]

In Dizqah et al. (2016) and in part of Lenzo et al. (2017a) a vehicle layout with four identical electric motors is considered (thus $a_{ij} = a$, $b_{ij} = b$, $c_{ij} = c$ and $d_{ij} = d$ in 83), and a further assumption is introduced, i.e., that the optimal wheel torque distribution is either:

- Single-Axle (SA): the whole side torque is allocated to a single wheel, i.e. either on the front wheel ($\sigma = 1$) or the rear wheel ($\sigma = 0$)—note that if the motors are identical, $\sigma = 0$ and $\sigma = 1$ yield the same power losses for a vehicle side
- Even-Distribution (ED): the side torque is evenly distributed between front and rear wheel ($\sigma = 0.5$)

On this basis, a "switching torque" $T_{sw}(V)$ is defined for each vehicle speed V as the side torque demand for which the SA and ED solutions are equivalent. Formally[25]:

$$P_{loss,1j}(T_{sw}, V) + P_{loss,2j}(0, V) = P_{loss,1j}(T_{sw}/2, V) + P_{loss,2j}(T_{sw}/2, V) \tag{84}$$

To calculate $T_{sw}(V)$, Lenzo et al. (2017a) propose two options: Hybrid Control Allocation (H-CA), where $T_{sw}(V)$ is calculated by interpolation of the experimental power loss curves; Explicit Control Allocation (E-CA), where $T_{sw}(V)$ is obtained through the analytical form 83, which combined with 84 gives

[24] These can be easily obtained imposing that the first order derivative of $P_{loss,ij}$ with respect to T_{ij} must be positive, and that the second order derivative is zero for a positive value of T_{ij}.

[25] Note that the left-hand side can be either $P_{loss,1j}(T_{sw}, V) + P_{loss,2j}(0, V)$ or $P_{loss,1j}(0, V) + P_{loss,2j}(T_{sw}, V)$ since, as discussed, $\sigma = 0$ and $\sigma = 1$ yield the same power losses for a vehicle side.

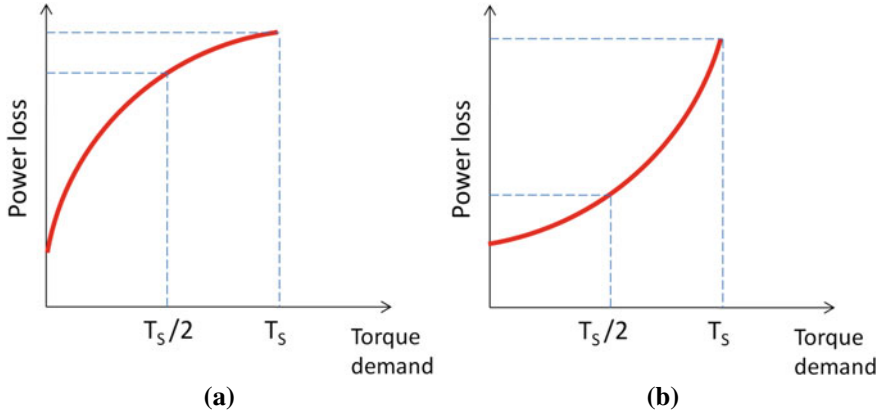

Fig. 14 Power loss functions of a single drivetrain for a given vehicle speed and side torque demand T_S. In case **a** $P_{loss}(T_S) < 2P_{loss}(T_S/2)$. In case **b** $P_{loss}(T_S) > 2P_{loss}(T_S/2)$

$$T_{sw}(V) = -\frac{2}{3}\frac{b}{a} \tag{85}$$

For both H-CA and E-CA the optimal solution is $\sigma = 1$ (or $\sigma = 0$[26]) if the side torque demand is lower than $T_{sw}(V)$, and $\sigma = 0.5$ when the side torque demand is greater than $T_{sw}(V)$. To give a more intuitive explanation, it is convenient to analyse the two extreme cases shown in Fig. 14:

- if the concavity is always negative, the optimal solution is to distribute the torque on one wheel only, SA, $\sigma = 0$ or $\sigma = 1$, as evidenced in Fig. 14a—in this case $T_{sw}(V) = \infty$;
- if the concavity is always positive, the optimal solution is the even distribution of the torque between front and rear motor, ED, $\sigma = 0.5$, as evidenced in Fig. 14b—in this case $T_{sw}(V) = 0$.

As discussed earlier, this approach assumed a-priori that the optimal torque distribution stategy is only either SA or ED (provided that the motors are all the same). It would be natural to wonder whether values of σ other than 0, 0.5 and 1 might be better. This was studied in Lenzo et al. (2017a) which propose the Implicit Control Allocation (I-CA). The I-CA basically assigns a specific value of σ for any combination of side torque demand and vehicle speed.

In terms of practical implementation on the vehicle, H-CA, E-CA and I-CA can easily be run in real time on hardware with low computational processing power, with the switching torque values (for H-CA and E-CA) or the σ map (for I-CA) simply stored as a look-up table in the controller.

[26] While $\sigma = 0$ and $\sigma = 1$ are equivalent in terms of power losses, $\sigma = 1$ is preferred for safety reasons since, from a vehicle dynamics point of view, understeer is better than oversteer.

Finally, it is worth to mention that Lenzo et al. (2017a):

- propose algorithms for the optimal distribution of wheel torque in case motors are not all the same;
- show that longitudinal and lateral load transfers, respectively due to longitudinal and lateral acceleration, only affect the term d_{ij} of the power losses but not the optimal front-to-total torque ratio, assuming that the rolling resistance depends linearly on the vertical load.

5.3 An Alternative for M_z: The Energy Efficiency Mode

As thoroughly discussed, M_z is an output of the high level controller which, in turn, uses the reference generator signals that are based on a desired driving mode. In the majority of the literature, driving modes are designed around appropriate vehicle handling requirements, which is the main priority. As a lower priority, the criterion of energy efficiency is addressed in the low level controller.

Another possibility, less explored in the literature, is to consider energy efficiency as the only target: in fact, M_z could be chosen based on energy requirements, too. Some recent works look at the design of understeer characteristics with the aim of improving energy efficiency (Lenzo et al., 2016; De Filippis et al., 2018). In De Filippis et al. (2018) a rule-based approach is proposed considering losses due to motor, inverter, transmission and longitudinal slip, along with the hypothesis of 4 identical and independent motors characterised by power losses expressed with the cubic polynomial function 83. For example, for low-medium values of longitudinal force (specifically, if $T_{tot} < 9/5T_{sw}$), the drivetrain power losses are minimised by a yaw moment that allocates the whole torque demand on either side of the vehicle. Actually, to minimise tyre slip power losses, too, the overall torque demand should be on the external side of the vehicle.[27] Another interesting consequence of the analysis in De Filippis et al. (2018) is that the optimal M_z is zero if the switching torque is zero, i.e. if the drivetrains are characterised by a convex shape for the whole range of torque demand.

In light of this, Mangia et al. (2021) propose an integrated torque vectoring framework including an "Energy efficiency" mode inspired to De Filippis et al. (2018), along with traditional "handling" driving modes such as those described in Sect. 3.2:

- When an "handling" driving mode is selected, M_z is imposed by the reference generator and the high level controller, and the low level controller manages σ_L and σ_R based on energy efficiency criteria.
- When the Energy efficiency mode is selected, the reference generator is bypassed and M_z, σ_L and σ_R are selected with the only target of minimising energy consumption.

[27] It is worth to note that, hypothetically, assigning more than the overall torque demand on the external vehicle side would imply a negative (regenerative) torque on the inner side, which is far from optimal (Lenzo et al., 2017a).

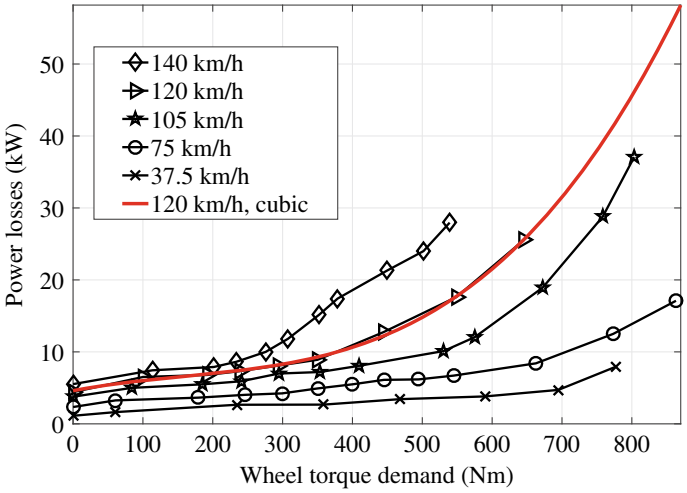

Fig. 15 Power losses of a single drivetrain for different vehicle speeds, and cubic interpolant for $V = 120$ km/h

Fig. 16 The experimental setup on the rolling road facility (reproduced from Lenzo et al., 2019b)

5.4 Experimental Results and Further Remarks

This section present a selection of relevant experimental results obtained within the European Project iCOMPOSE (Lenzo et al., 2019b), with the vehicle demonstrator seen in Sect. 4.3.

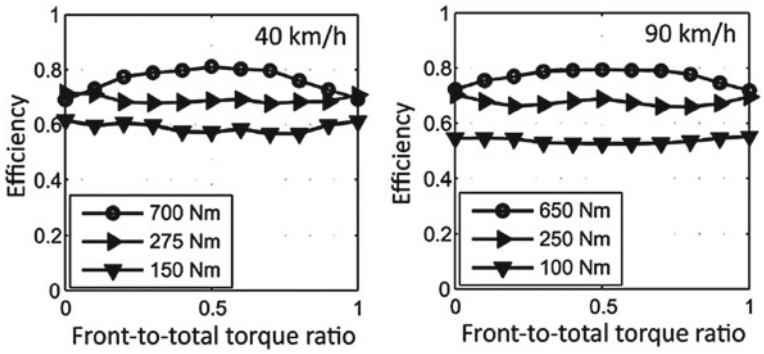

Fig. 17 Measured drivetrain efficiencies as a function of σ for different side torques and vehicle speeds of 40 and 90 km/h

Figure 15 shows the power losses of a single drivetrain as a function of the torque demand for different vehicle speeds, obtained through extensive experimental tests on a MAHA rolling road facility (Fig. 16). To demonstrate the effectiveness of the function 83, Fig. 15 also shows the interpolating function for a sample vehicle speed.

Figure 17 shows the measured drivetrain efficiency (i.e., the ratio bewteen mechanical power output, measured at the MAHA rollers, and electrical power input) of the drivetrain for two selected speeds and various torque demands: as discussed earlier, for low torque demands $\sigma = 0$ or $\sigma = 1$ are better than $\sigma = 0.5$, and vice-versa for sufficiently high torque demands. The switching torque, T_{sw}, is depicted in Fig. 18a which shows the results of the calculations via piecewise interpolation (H-CA) and via the analytical expression 85 (E-CA). Figure 18b shows the I-CA map: interestingly, the blue curve of Fig. 18a overlaps rather well with the transition zone between white and dark grey of Fig. 18b. This is not a surprise since the idea of the H-CA and E-CA strategy (i.e., use $\sigma = 1$ below T_{sw} and $\sigma = 0.5$ above T_{sw}) is an approximation of the I-CA.

The benefit of H-CA, E-CA and I-CA was assessed through the measurement of the energy input required for several driving cycles including, e.g., New European Driving Cycle (NEDC), Artemis Road, etc. Results[28] showed that generally H-CA, E-CA and I-CA outperform SA and ED by between 2 and 4%. While the I-CA is in principle better than H-CA and E-CA because it uses the whole range $0 \leq \sigma \leq 1$, experiments showed that not only the energy consumption improvements of the I-CA were hardly significant, but that practically the continuous variation of the torque distribution between front and rear axle provokes undesired vehicle vibrations which seriously hinder drivability and comfort. Between H-CA and E-CA, the former is recommended as it provides slightly better results than the E-CA, simply because of the more accurate approximation of the power losses and the switching torque. Additionally, despite these CA strategies are not explicitly designed for cornering

[28] Details are in Lenzo et al. (2017a).

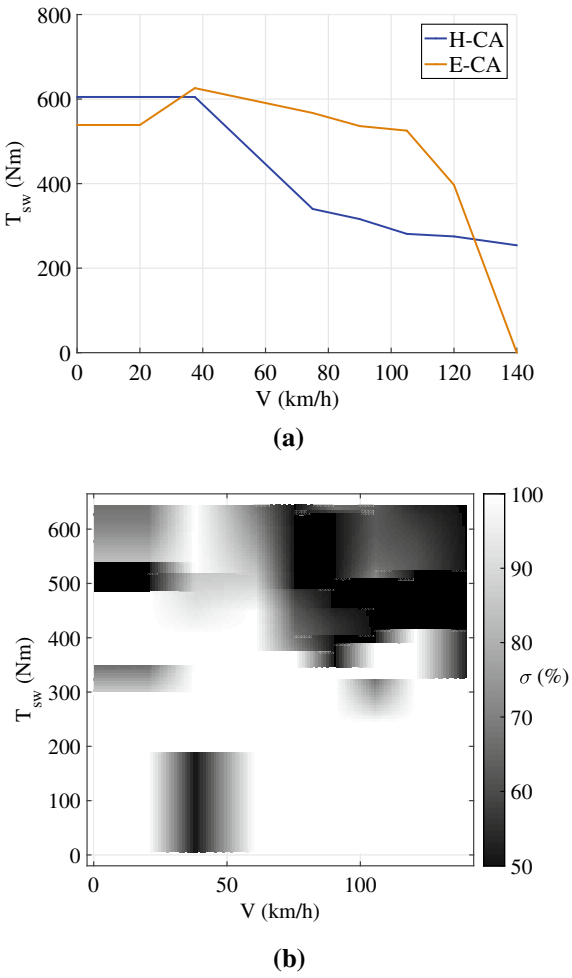

Fig. 18 Elaboration of the power losses shown in Fig. 15: **a** switching torque using the H-CA and the E-CA; **b** σ map for the I-CA

conditions, skid-pad tests were executed for lateral accelerations between 2 and 8 m/s^2, and the H-CA brought experimentally measured energy savings of up to 5% with respect to the SA and ED strategies.

Regarding the energy consumption benefits achieved through the design of the reference cornering response of the vehicle, several experimental skidpad tests were conducted. As a result, it was found that for the case-study vehicle the optimal cornering response in terms of energy efficiency is close to the neutral steering condition, and can reduce the measured inverter input power by even more than 10% (Fig. 19).

It should also be noted that the driving style has a large impact on power consumption, too: energy efficiency optimisation algorithms cannot be much effective if associated with an aggressive driving style.

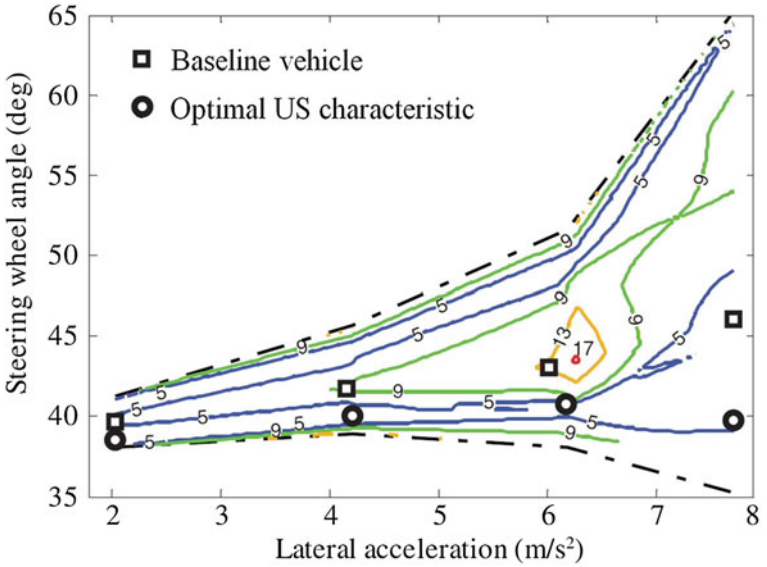

Fig. 19 Understeer diagram with indication of the relative power input increase (in percentage) with respect to the optimal understeer characteristic (reproduced from Lenzo et al., 2019b)

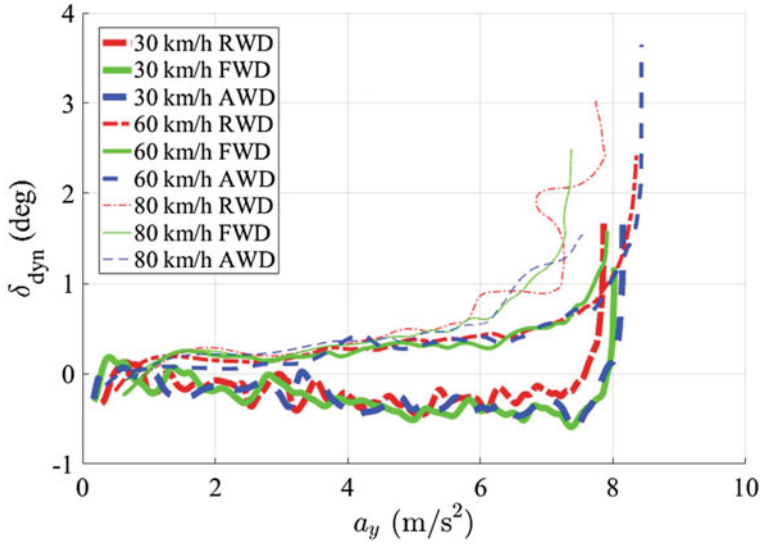

Fig. 20 Dynamic steering angle as a function of the lateral acceleration (reproduced from Lenzo et al., 2019b)

An important practical remark for onboard motor configurations is that potential fast modulations of the motor torque during transients might lead to drivability and possibly yaw stability problems. To solve this issue, De Novellis et al. (2015b) developed a specific anti-jerk control function, called Active Vibration Controller (AVC). Essentially its effect corresponds to the one of a virtual damper between the wheel to the electric drivetrain. As a consequence, the AVC is based on the difference (reported to the same shaft) between motor speed and wheel speed:

$$T_{ij,AVC} = T_{ij} - c_{AVC}(\dot{\omega}_{ij} - \dot{\omega}_{w,ij}/\tau) \tag{86}$$

where $T_{ij,AVC}$ is the torque demand actually sent to the wheel by the AVC, ω_{ij} is the angular speed of motor ij, $\omega_{w,ij}$ is the angular speed of wheel ij, c_{AVC} is a tuning factor, τ is the overall gear ratio.

A further interesting aspect of the vehicle demonstrator used in iCOMPOSE is that it allowed to emulate architectures such as Front Wheel Drive (FWD), Rear Wheel Drive (RWD) and All Wheel Drive (AWD) by simply changing the vehicle control settings. This inspired a study (Lenzo et al., 2019a) on the effect of the front-to-rear wheel torque distribution on the handling behaviour, with $M_z = 0$. In other words, it was possible to compare a FWD, RWD and AWD layouts with the very same equipment. Interestingly, the study showed that at low speed and high lateral acceleration, the RWD vehicle is more understeering than the FWD and the AWD ones (Fig. 20). This intuitively unexpected result was discussed and justified by a thorough analysis of the yaw moment contributions caused by the longitudinal forces of the front tyres (N_f in 50).

References

Acosta, M., & Kanarachos, S. (2018). Tire lateral force estimation and grip potential identification using neural networks, extended kalman filter, and recursive least squares. *Neural Computing and Applications, 30*(11), 3445–3465.

Åström, K. J., & Murray, R. M. (2010). *Feedback systems: An introduction for scientists and engineers*. Princeton University Press.

Bucchi, F., & Frendo, F. (2016). A new formulation of the understeer coefficient to relate yaw torque and vehicle handling. *Vehicle System Dynamics, 54*(6), 831–847.

Cheli, F., Sabbioni, E., Pesce, M., & Melzi, S. (2007). A methodology for vehicle sideslip angle identification: Comparison with experimental data. *Vehicle System Dynamics, 45*(6), 549–563.

Chen, L., Chen, T., Xing, X., Cai, Y., Jiang, H., & Sun, X. (2018). Multi-objective coordination control strategy of distributed drive electric vehicle by orientated tire force distribution method. *IEEE Access, 6,* 69559–69574.

Chindamo, D., Lenzo, B., & Gadola, M. (2018). On the vehicle sideslip angle estimation: A literature review of methods, models, and innovations. *Applied Sciences, 8*(3), 355.

De Filippis, G., Lenzo, B., Sorniotti, A., Sannen, K., De Smet, J., & Gruber, P. (2016). On the energy efficiency of electric vehicles with multiple motors. In *2016 IEEE Vehicle Power and Propulsion Conference (VPPC)* (pp. 1–6). IEEE.

De Filippis, G., Lenzo, B., Sorniotti, A., Gruber, P., & De Nijs, W. (2018). Energy-efficient torque-vectoring control of electric vehicles with multiple drivetrains. *IEEE Transactions on Vehicular Technology*.

De Novellis, L., Sorniotti, A., & Gruber, P. (2013). Optimal wheel torque distribution for a four-wheel-drive fully electric vehicle. *SAE International Journal of Passenger Cars-Mechanical Systems, 6*(2013-01-0673), 128–136.

De Novellis, L., Sorniotti, A., & Gruber, P. (2014a). Design and comparison of the handling performance of different electric vehicle layouts. *Proceedings of the Institution of Mechanical Engineers, Part D: Journal of Automobile Engineering, 228*(2), 218–232.

De Novellis, L., Sorniotti, A., & Gruber, P. (2014b). Wheel torque distribution criteria for electric vehicles with torque-vectoring differentials. *IEEE Transactions on Vehicular Technology, 63*(4), 1593–1602.

De Novellis, L., Sorniotti, A., Gruber, P., & Pennycott, A. (2014c). Comparison of feedback control techniques for torque-vectoring control of fully electric vehicles. *IEEE Transactions on Vehicular Technology, 63*(8), 3612–3623.

De Novellis, L., Sorniotti, A., & Gruber, P. (2015a). Driving modes for designing the cornering response of fully electric vehicles with multiple motors. *Mechanical Systems and Signal Processing, 64,* 1–15.

De Novellis, L., Sorniotti, A., Gruber, P., Orus, J., Rodriguez Fortun, J.-M., Theunissen, J., & De Smet, J. (2015b). Theoretical design and experimental assessment. Direct yaw moment control actuated through electric drivetrains and friction brakes. *Mechatronics, 26*, 1–15.

Ding, S., Liu, L., & Zheng, W. X. (2017). Sliding mode direct yaw-moment control design for in-wheel electric vehicles. *IEEE Transactions on Industrial Electronics, 64*(8), 6752–6762.

Dizqah, A. M., Lenzo, B., Sorniotti, A., Gruber, P., Fallah, S., & De Smet, J. (2016). A fast and parametric torque distribution strategy for four-wheel-drive energy-efficient electric vehicles. *IEEE Transactions on Industrial Electronics, 63*(7), 4367–4376.

Esmailzadeh, E., Goodarzi, A., & Vossoughi, G. R. (2003). Optimal yaw moment control law for improved vehicle handling. *Mechatronics, 13*(7), 659–675.

Frendo, F., Greco, G., Guiggiani, M., & Sponziello, A. (2007). The handling surface: A new perspective in vehicle dynamics. *Vehicle System Dynamics, 45*(11), 1001–1016.

Gasmi, A., Boudali, M.-T., Orjuela, R., & Basset, M. (2019). Multi-criteria stability combination for yaw stability control of autonomous vehicles. *IFAC-PapersOnLine, 52*(5), 465–470.

Genta, G. (1997). *Motor vehicle dynamics: Modeling and simulation* (Vol. 43). World Scientific.

Goggia, T., Sorniotti, A., De Novellis, L., Ferrara, A., Gruber, P., Theunissen, J., et al. (2015). Integral sliding mode for the torque-vectoring control of fully electric vehicles: Theoretical design and experimental assessment. *IEEE Transactions on Vehicular Technology, 64*(5), 1701–1715.

Gruber, P., Sorniotti, A., Lenzo, B., De Filippis, G., & Fallah, S. (2016). Energy efficient torque vectoring control. *Advanced vehicle control AVEC* (pp. 17–22). CRC Press.

Guiggiani, M. (2018). *The science of vehicle dynamics*. Springer.

Guo, H., Cao, D., Chen, H., Lv, C., Wang, H., & Yang, S. (2018). Vehicle dynamic state estimation: State of the art schemes and perspectives. *IEEE/CAA Journal of Automatica Sinica, 5*(2), 418–431.

Guo, N., Lenzo, B., Zhang, X., Zou, Y., Zhai, R., & Zhang, T. (2020). A real-time nonlinear model predictive controller for yaw motion optimization of distributed drive electric vehicles. *IEEE Transactions on Vehicular Technology, 69*(5), 4935–4946.

He, J.-B., Wang, Q.-G., & Lee, T.-H. (2000). PI/PID controller tuning via LQR approach. *Chemical Engineering Science, 55*(13), 2429–2439.

Isermann, R. (2012). *Digital control systems: Volume 2: Stochastic control, multivariable control, adaptive control, applications*. Springer Science & Business Media.

Kaiser, G. (2015). *Torque vectoring-linear parameter-varying control for an electric vehicle*. Technische Universität Hamburg.

Kiencke, U., & Nielsen, L. (2000). *Automotive control systems: For engine, driveline, and vehicle*.

Koehler, S., Viehl, A., Bringmann, O., & Rosenstiel, W. (2015). Improved energy efficiency and vehicle dynamics for battery electric vehicles through torque vectoring control. In *2015 IEEE Intelligent Vehicles Symposium (IV)* (pp. 749–754). IEEE.

Lenzo, B., & De Castro, R. (2019). Vehicle sideslip estimation for four-wheel-steering vehicles using a particle filter.

Lenzo, B., Sorniotti, A., De Filippis, G., Gruber, P., & Sannen, K. (2016). Understeer characteristics for energy-efficient fully electric vehicles with multiple motors. In *EVS29 International Battery, Hybrid and Fuel Cell Electric Vehicle Symposium Proceedings*.

Lenzo, B., De Filippis, G., Moradinegade Dizqah, A., Sorniotti, A., Gruber, P., Fallah, S., & De Nijs, W. (2017a). Torque distribution strategies for energy-efficient electric vehicles with multiple drivetrains. *Journal of Dynamic Systems, Measurement, and Control, 139*(12).

Lenzo, B., Sorniotti, A., Gruber, P., & Sannen, K. (2017b). On the experimental analysis of single input single output control of yaw rate and sideslip angle. *International Journal of Automotive Technology, 18*(5), 799–811.

Lenzo, B., Bucchi, F., Sorniotti, A., & Frendo, F. (2019a). On the handling performance of a vehicle with different front-to-rear wheel torque distributions. *Vehicle System Dynamics, 57*(11), 1685–1704.

Lenzo, B., Gruber, P., & Sorniotti, A. (2019b). On the enhancement of vehicle handling and energy efficiency of electric vehicles with multiple motors: The icompose project. In *The IAVSD International Symposium on Dynamics of Vehicles on Roads and Tracks* (pp. 1342–1349). Springer.

Lenzo, B., Zanchetta, M., Sorniotti, A., Gruber, P., & De Nijs, W. (2021). Yaw rate and sideslip angle control through single input single output direct yaw moment control. *IEEE Transactions on Control Systems Technology*.

Lin, C., & Zhifeng, X. (2015). Wheel torque distribution of four-wheel-drive electric vehicles based on multi-objective optimization. *Energies, 8*(5), 3815–3831.

Qian, L., Sorniotti, A., Gruber, P., Theunissen, J., & De Smet, J. (2016). H-infinity loop shaping for the torque-vectoring control of electric vehicles: Theoretical design and experimental assessment. *Mechatronics, 35,* 32–43.

Mahmoudi, A., Soong, W. L., Pellegrino, G., & Armando, E. (2015). Efficiency maps of electrical machines. In *2015 IEEE Energy Conversion Congress and Exposition (ECCE)* (pp. 2791–2799). IEEE.

Mangia, A., Lenzo, B., & Sabbioni, E. (2021). An integrated torque-vectoring control framework for electric vehicles featuring multiple handling and energy-efficiency modes selectable by the driver. *Meccanica*, 1–20.

Manning, W. J., & Crolla, D. A. (2007). A review of yaw rate and sideslip controllers for passenger vehicles. *Transactions of the Institute of Measurement and Control, 29*(2), 117–135.

Pacejka, H. (2006). *Tire and vehicle dynamics*. Butterworth-Heinemann.

Parra, A., Zubizarreta, A., Pérez, J., & Dendaluce, M. (2018). Intelligent torque vectoring approach for electric vehicles with per-wheel motors. *Complexity, 2018*.

Pennycott, A., De Novellis, L., Gruber, P., & Sorniotti, A. (2015). Sources of power loss during torque-vectoring for fully electric vehicles. *International Journal of Vehicle Design, 67*(2), 157–177.

Piyabongkarn, D., Lew, J. Y., Rajamani, R., & Grogg, J. A. (2010). Active driveline torque-management systems. *IEEE Control Systems Magazine, 30*(4), 86–102.

Preda, I., Covaciu, D., & Ciolan, G. (2010). Coast down test–theoretical and experimental approach.

Rajamani, R. (2011). *Vehicle dynamics and control*. Springer Science & Business Media.

Sforza, A., Lenzo, B., & Timpone, F. (2019). A state-of-the-art review on torque distribution strategies aimed at enhancing energy efficiency for fully electric vehicles with independently actuated drivetrains. *International Journal of Mechanics and Control, 20*(2), 3–15.

Siampis, E., Velenis, E., & Longo, S. (2016). Front-to-rear torque vectoring model predictive control for terminal understeer mitigation. In *The Dynamics of Vehicles on Roads and Tracks: Proceedings of the 24th Symposium of the International Association for Vehicle System Dynamics (IAVSD 2015)*, Graz, Austria, 17–21 August 2015 (p. 153). CRC Press.

Skogestad, S., & Postlethwaite, I. (2007). *Multivariable feedback control: Analysis and design* (Vol. 2). New York: Wiley.

Stanford-University (2020). *Linear quadratic regulator*. Retrieved June 09, 2020, from https://stanford.edu/class/ee363/lectures/dlqr.pdf

Tota, A., Lenzo, B., Qian, L., Sorniotti, A., Gruber, P., Fallah, S., et al. (2018). On the experimental analysis of integral sliding modes for yaw rate and sideslip control of an electric vehicle with multiple motors. *International Journal of Automotive Technology, 19*(5), 811–823.

Tuncay, R. N., Ustun, O., Yilmaz, M., Gokce, C., & Karakaya, U. (2011). Design and implementation of an electric drive system for in-wheel motor electric vehicle applications. In *2011 IEEE Vehicle Power and Propulsion Conference* (pp. 1–6). IEEE.

Utkin, V., & Shi, J. (1996). Integral sliding mode in systems operating under uncertainty conditions. In *Proceedings of 35th IEEE Conference on Decision and Control* (Vol. 4, pp. 4591–4596). IEEE.

Utkin, V., Guldner, J., & Shi, J. (2017). *Sliding mode control in electro-mechanical systems*. CRC Press.

Vantsevich, V. V., Barz, D., Kubler, J., & Schumacher, A. (2005). Tire longitudinal elasticity and effective rolling radii: Experimental method and data. Technical report, SAE Technical Paper.

Vantsevich, V. V., Paldan, J., & Verma, M. (2017). Instantaneous compression-based tyre rolling radius. In *Dynamics of Vehicles on Roads and Tracks Vol 1: Proceedings of the 25th International Symposium on Dynamics of Vehicles on Roads and Tracks (IAVSD 2017)*, 14–18 August 2017, Rockhampton, Queensland, Australia (p. 259). CRC Press.

Vignati, M., Sabbioni, E., & Tarsitano, D. (2016). Torque vectoring control for IWM vehicles. *International Journal of Vehicle Performance, 2*(3), 302–324.

Wang, J., Gao, S., Wang, K., Wang, Y., & Wang, Q. (2021). Wheel torque distribution optimization of four-wheel independent-drive electric vehicle for energy efficient driving. *Control Engineering Practice, 110*, 104779.

White, R. A., & Korst, H. H. (1972). The determination of vehicle drag contributions from coast-down tests. *SAE Transactions*, 354–359.

Wong, A., Kasinathan, D., Khajepour, A., Chen, S.-K., & Litkouhi, B. (2016). Integrated torque vectoring and power management framework for electric vehicles. *Control Engineering Practice, 48,* 22–36.

Zanchetta, M., Tavernini, D., Sorniotti, A., Gruber, P., Lenzo, B., Ferrara, A., Sannen, K., De Smet, J., & De Nijs, W. (2019). Trailer control through vehicle yaw moment control: Theoretical analysis and experimental assessment. *Mechatronics,64*, 102282.

Zhou, H., & Liu, Z. (2009). Design of vehicle yaw stability controller based on model predictive control. In *2009 IEEE Intelligent Vehicles Symposium* (pp. 802–807). IEEE.